HHS Public Access

Author manuscript

Nat Immunol. Author manuscript; available in PMC 2020 November 18.

Published in final edited form as:

Nat Immunol. 2020 July ; 21(7): 790–801. doi:10.1038/s41590-020-0678-5.

Infection-induced plasmablasts are a nutrient sink that impairs humoral immunity to malaria

Rahul Vijay[1,10], **Jenna J. Guthmiller**[2,8,10], **Alexandria J. Sturtz**[1], **Fionna A. Surette**[1,3], **Kai J. Rogers**[1], **Ramakrishna R. Sompallae**[4], **Fengyin Li**[1,9], **Rosemary L. Pope**[2], **Jo-Anne Chan**[5], **Fabian de Labastida Rivera**[6], **Dean Andrew**[6], **Lachlan Webb**[6], **Wendy J. Maury**[1,3], **Hai-Hui Xue**[1,3,7], **Christian R. Engwerda**[6], **James S. McCarthy**[6], **Michelle J. Boyle**[5,6], **Noah S. Butler**[1,2,3]

[1]Department of Microbiology and Immunology, The University of Iowa, Iowa City, Iowa, USA.

[2]Department of Microbiology and Immunology, University of Oklahoma Health Sciences Center Oklahoma City, Oklahoma, USA.

[3]Interdisciplinary Graduate Program in Immunology, The University of Iowa, Iowa City, Iowa, USA.

[4]Department of Pathology, The University of Iowa, Iowa City, Iowa, USA.

[5]Burnet Institute, Melbourne, Victoria, Australia.

[6]QIMR Berghofer Medical Research Institute, Herston, Queensland, Australia.

[7]Iowa City Veterans Affairs Health Care System, Iowa City, Iowa, USA

[8]Current Address: Department of Medicine, Section of Rheumatology, The University of Chicago, Chicago, Illinois.

[9]Current Address: Division of Life Science and Medicine, University of Science and Technology of China, Hefei, China.

[10]Co-lead authors

Abstract

Plasmodium parasite-specific antibodies are critical for protection against malaria, yet the development of long-lived and effective humoral immunity against *Plasmodium* takes many years and multiple rounds of infection and cure. Here we report that the rapid development of short-lived

Correspondence: Noah S. Butler, Ph.D., Department of Microbiology and Immunology, University of Iowa, Iowa City, Iowa 52242, noah-butler@uiowa.edu.

Author Contributions

R.V., J.J.G. and N.S.B. conceptualized the project. J.J.G. performed foundational studies and characterized the phenotype of plasmablasts in mice. R.V. characterized the transcriptome of the plasmablasts as well as conceived and executed the adoptive transfer studies, chimeric studies, metabolism analyses, and glutamine supplementation experiments. W.J.M., K. J. R., F.L. and H.-H.X. provided critical reagents and technical assistance. C.R.E., J.S.M. and M.J.B. supervised the clinical studies. N.S.B. supervised the experimental rodent studies. R.V., J.J.G., H.-H.X., C.R.E., J.S.M., M.J.B. and N.S.B. designed the experiments. R.V., J.J.G., A.J.S., F.A.S., R.L.P., D. A., J-A.C. and F.L.R. performed the experiments. R.V., J.J.G., A.J.S., F.A.S., R.R.S., J-A.C., F.L.R., L.W., C.R.E., J.S.M., M.J.B. and N.S.B. analyzed the data. R.V. and R.R.S. performed the bioinformatic analyses. R.V. and J.J.G. made the figures. R.V. wrote the original draft. J.J.G., A.J.S., C.R.E., J.S.M., M.J.B. and N.S.B. reviewed and edited the manuscript and figures.

Competing interests. None.

plasmablasts during experimental malaria unexpectedly hindered parasite control by impeding germinal center (GC) responses. Metabolic hyperactivity of plasmablasts resulted in nutrient deprivation of the GC reaction limiting the generation of memory B cell and long-lived plasma cell responses. Therapeutic administration of a single amino acid to experimentally infected mice was sufficient to overcome the metabolic constraints imposed by plasmablasts and enhanced parasite clearance and the formation of protective humoral immune memory responses. Thus, our studies not only challenge the current paradigm describing the role and function of blood-stage *Plasmodium*-induced plasmablasts, but also reveal new targets and strategies to improve anti-*Plasmodium* humoral immunity.

Keywords

Plasmodium; malaria; plasmablasts; glutamine; metabolism; germinal center; humoral immunity; immunosuppression

Introduction

Following either vaccination or microbial infection, humoral immunity generally consists of temporally and spatially layered B cell activation events. Early humoral responses are associated with extrafollicular B cells that proliferate and rapidly differentiate into short-lived antibody secreting cells (ASCs), also referred to as plasmablasts[1]. T cell-dependent follicular responses take longer to develop and involve antigen-specific B cells forming a germinal center (GC) where they engage in sustained interactions with $CD4^+$ T follicular helper cells (T_{FH}). GC B cells subsequently differentiate into either memory B cells (MBCs) or long-lived plasma cells (LLPCs) that secrete high-affinity, class-switched antibodies[1, 2]. It is thought that extrafollicular, short-lived plasmablasts limit pathogen dissemination[3, 4] until LLPC and MBC responses develop, which act to resolve the primary infection and mediate resistance to subsequent pathogen exposures[5].

Plasmodium infections caused an estimated 219 million cases of malaria and resulted in approximately 435,000 deaths in 2017[6]. Both clinical and experimental studies identify *Plasmodium*-specific antibodies as critical for both limiting disease severity and promoting clearance of blood-stage parasites[7]. Although durable immunity to either *P. vivax* or *P. falciparum* has been reported in travelers and individuals from areas of relatively low transmission intensity[8, 9, 10], in regions of high *P. falciparum* transmission, parasite-specific LLPCs and MBCs are not efficiently induced and sterilizing immunity against blood-stage *P. falciparum* is seldom acquired, even following repeated infections[11, 12].

Multiple mechanisms have been postulated to explain the short-lived nature of *Plasmodium*-specific humoral immune responses, including preferential expansion of $CXCR3^+$ (T_H1-like) T_{FH} cells[13], regulatory T cells[14, 15] and atypical MBCs[16, 17, 18, 19], as well as the dysregulation of chemokines and cytokines[20, 21] and induction of immune checkpoints[22, 23] that may delay or impair the acquisition of humoral immunity against malaria. Although these studies have identified numerous mechanisms that may contribute to the lack of durable immunity against malaria, our past studies showed that genetic manipulations that either expand or constrain the *Plasmodium*-specific GC response[24] are associated with

substantially blunted or elevated plasmablast responses, respectively (Guthmiller and Butler, unpublished observations). These data raise the possibility that blood-stage *Plasmodium* infections may preferentially induce immunosuppressive plasmablast populations that reduce the development of GC B cell responses and the induction of long-lived humoral immunity. Herein, we used combinations of clinical trials and experimental rodent malaria models to define the dynamics of infection-induced plasmablast populations and interrogate their contribution to anti-*Plasmodium* immunity. Our data show that clinical and experimental blood-stage *Plasmodium* infection preferentially expands short-lived plasmablast populations and that during experimental malaria these cells may function as a metabolic sink that constrains GC-derived humoral immune reactions, thereby identifing a previously unknown mechanism by which *Plasmodium* parasites subvert host immunity.

Results

Plasmablasts dominate the response to *Plasmodium* infection

To examine the kinetics and magnitude of splenic ASC/plasmablast responses during experimental malaria, we infected wild-type C57BL/6 mice with *Plasmodium yoelii* (*Py*) strain 17XNL parasitized red blood cells (pRBCs). This infection is normally non-lethal to wild-type C57BL/6 mice and it mimics aspects of severe anemia and hyperparasitemia associated with *P. falciparum* infection of malaria-naïve individuals. We quantified activated and/or class-switched (IgD^{neg}) $CD19^{+}$ B cells that expressed the adhesion and migratory factor CD138 (syndecan-1) (Extended Data Fig. 1a). Both splenic (Fig. 1a) and circulating (Extended Data Fig. 1b) $CD138^{hi}IgD^{neg}$ plasmablast populations numerically peaked on day 10 post-infection (p.i.), underwent rapid contraction and returned to pre-infection numbers in the spleen by day 28 p.i. Notably, approximately 60–80% of all activated (IgD^{neg}) splenic B cells displayed characteristics of $CD138^{hi}$ plasmablasts on day 10 p.i. By comparison, blood-stage *Py* infection-induced splenic GC ($B220^{+}GL7^{+}CD95^{+}$) B cell responses slowly accumulated through day ~21 p.i. and persisted after parasite clearance (Fig. 1b), as previously described [25]. As expected, blood-stage *Py* infection-induced $CD138^{hi}$ B cells uniformly expressed Blimp-1 (Fig. 1c), a transcriptional repressor encoded by *Prdm1* that is essential for plasmablast development[26]. $CD138^{hi}$ plasmablast populations also secreted either IgM or IgG and at least a fraction of the cells reacted with *Py*-infected RBC lysate antigen (Fig. 1d,e and Extended Data Fig. 1c). Relative to $CD138^{lo}CD19^{hi}$ B cells, $CD138^{hi}$ plasmablasts also retained intermediate expression of CD19 (Extended Data Fig. 1d), unlike LLPCs that fully down-regulate CD19[26]. $CD138^{hi}$ plasmablasts or their precursors incorporated 5-bromodeoxyuridine (BrdU) between days 6–10 p.i. (Extended Data Fig. 1e) and the cells exhibited higher forward scatter (Extended Data Fig. 1f), both of which are characteristics of proliferating/blasting cells. In agreement with the notion that these cells are actively engaged in antibody synthesis, $CD138^{hi}$ plasmablasts exhibited extensive rough endoplasmic reticulum (Fig. 1f). At the peak of the response on day 10 p.i., ~40% of $CD138^{hi}$ plasmablasts exhibited caspase-3 and −7 activation (Fig. 1g) and by day 21 p.i., the number of $CD138^{hi}$ plasmablasts in the bone marrow was similar to that in naïve mice (Extended Data Fig. 1g), suggesting that their disappearance from the spleen and blood may be linked to apoptosis and was unlikely due to rapid migration of $CD138^{hi}$ plasmablasts to the bone marrow.

The spleen contains a heterogeneous population of B lymphocytes that includes follicular (FO, $CD21^{int}CD23^{+}$) and marginal zone (MZ, $CD21^{hi}CD23^{neg}$) B cells (Extended Data Fig. 1h). Splenic $CD138^{hi}$ plasmablasts are reported to differentiate from either FO or MZ B cells[27]. We found that $CD138^{hi}$ plasmablasts did not exhibit characteristics of FO B cells and only a minor proportion (~15%) exhibited characteristics of MZ B cells, whereas blood-stage *Py* infection-induced activated ($CD138^{lo}IgD^{neg}$) B cells and the bulk of resting ($CD138^{lo}IgD^{hi}$) B cells displayed characteristics of either FO or MZ B cells (Extended Data Fig. 1i). $CD138^{hi}$ plasmablasts also did not express markers of GC B cells ($GL\text{-}7^{+}Fas^{+}$) (Extended Data Fig. 1j). In agreement with this surface phenotype, the majority of blood-stage *Plasmodium* infection-induced $CD138^{hi}$ plasmablasts localized outside of B cell follicles (Fig. 1h). Together, these data support that blood-stage *Plasmodium* infection is associated with transient yet substantial accumulations of $CD138^{hi}IgD^{neg}$ plasmablasts that localize outside of follicles.

$CD138^{hi}$ plasmablasts constrain anti-*Plasmodium* humoral immunity

The significant expansion and accumulation of $CD138^{hi}$ plasmablasts suggests they may play a critical role in mediating host protection against blood-stage *Plasmodium* infection. To test this hypothesis, we first transferred $CD138^{hi}$ plasmablasts purified from *Py*-infected donors to *Py*-infected recipient mice 5 days before the peak of the endogenous $CD138^{hi}$ plasmablast response in recipients (Extended Data Fig. 2a). Notably, transfer of $CD138^{hi}$ plasmablasts resulted in higher parasite burdens (Fig. 2a), compared to recipients receiving either activated ($CD138^{lo}IgD^{neg}$) B cells or PBS. Recipients of $CD138^{hi}$ plasmablast also exhibited lower titers of parasite lysate-specific IgG2b on day 21 p.i. (day 16 post-transfer) (Fig. 2b). Next, we employed a genetic approach focused on *Prdm1*. We generated competitive mixed bone marrow chimeric mice in which we could conditionally and selectively delete *Prdm1* from the B cell compartment (Extended Data Fig. 2b). Tamoxifen treatment of *Py*-infected Cre^{+} chimeric mice abrogated $CD138^{hi}$ plasmablast responses (Fig. 2c) and enhanced parasite control (Fig. 2d). Genetic blockade of plasmablast development also resulted in 8 to 10-fold increases in number of GC B cells (Fig. 2e) and GC-T_{FH}-like cells (Fig. 2f and Extended Data Fig. 2c) and higher titers of merozoite surface protein 1 ($MSP1_{19}$)-specific serum IgG2b (Fig. 2g). Importantly, tamoxifen had no effect on parasite growth when administered to either *Py*-infected Cre^{neg} chimeric (not shown) or wild-type mice (Extended Data Fig. 2d) and inducible deletion of *Prdm1* did not instead simply skew B cell differentiation towards the GC fate in *Py*-infected chimeric mice (Extended Data Fig. 2e,f).

Although elevated parasite-specific antibody titers and enhanced parasite control were somewhat unexpected in the absence of Blimp-1, previous studies showed that antigen-specific IgG secretion is only modestly reduced in splenic B cell subsets lacking *Prdm1*[28]. However, early production of natural killer cell- and T_H1-derived IFN-γ can suppress *Plasmodium* replication early after blood-stage infection[29, 30] and we observed 2-fold increases in $Ly6C^{+}CXCR3^{+}IFN\text{-}\gamma^{+}$ T_H1-like cell responses in tamoxifen-treated, *Py*-infected Cre^{+} chimeric mice (Extended Data Fig. 2g). These data support that blood-stage *Py* infection-induced $CD138^{hi}$ plasmablasts suppress GC responses and constrain anti-*Plasmodium* humoral immunity.

Deletion of plasmablasts improves humoral immunity

To confirm the effects of abrogating the CD138^{hi} plasmablast response without impacting GC-derived plasma cell responses, we generated CD138-DTR bone marrow chimeric mice in which CD138^{+} hematopoietic cells could be deleted using diphtheria toxin (DTx) (Extended Data Fig. 3a). Importantly, this approach deletes plasmablasts and plasma cells at the time of treatment, but allows the development of future LLPCs. DTx-mediated deletion of CD138^{hi} plasmablasts (Fig. 3a) in *Py*-infected chimeric mice resulted in decreased parasite burden (Fig. 3b), increases in both the number of GC B cells (Fig. 3c) and GC-T_{FH}-like cells (Fig. 3d), as well as elevated serum titers of $MSP1_{19}$-specific IgG (Fig. 3e) on day 21 p.i. Concomitant with the loss of CD138^{hi} plasmablasts, DTx-treatment transiently reduced the number of splenic ASCs on day 10 p.i. However, numbers of splenic ASC were elevated on days 15 and 21 p.i. in DTX-treated mice (Fig. 3f,g), perhaps as a result of GC-derived ASC formation. No differences in either parasite burden, GC B cells or GC-T_{FH}-like cells were observed when *Py*-infected wild-type mice were treated with DTx (Extended Data Fig. 3b–d). Thus, reduced parasite loads and elevated GC responses in DTx-treated CD138-DTR chimeric mice were a consequence of CD138^{hi} plasmablast deletion, and not due to any direct effect of DTx on parasite growth or immune cell activation.

In order to examine whether the improved parasite control in DTx-treated CD138-DTR chimeric mice was linked to enhanced GC responses, we distrupted CD4 T cell-mediated co-stimulation by adminstering CD40L blocking antibody (clone MR1) on days 8–11 p.i. Anti-CD40L treatment of DTx-treated mice reduced the frequency and numbers of GC B and GC-T_{FH}-like cells by 3 to 5-fold and fully abrogated parasite control (Extended Data Fig. 3e–g). Taken together, these cellular, biochemical and genetic manipulations support that blood-stage *Py* infection-induced CD138^{hi} plasmablasts suppress GC responses and contribute to increased parasite burden during the acute phase of experimental malaria.

CD138^{hi} plasmablasts are metabolically hyperactive

To gain insight into the potential mechanisms by which blood-stage *Py*-induced CD138^{hi} plasmablasts constrain GC responses, we performed RNA-seq analysis on splenic CD138^{hi} plasmablasts, as well as activated (CD138^{lo}IgD^{neg}) and resting (CD138^{lo}IgD^{hi}) B cell populations that are each present on day 10 p.i. (Fig. 4a). Principal component analysis (PCA) revealed that the three populations of B cells clustered distinctly from each other (Fig. 4b) with resting and activated B cells more similar to each other than CD138^{hi} plasmablasts (Extended Data Fig. 4a,b and Supplementary Table 1). Of the 3600 genes that were differentially expressed among the populations, multiple metabolism-related genes that play pivotal roles in the glycolytic and citric acid cycle pathways were distinctly expressed in CD138^{hi} plasmablasts, compared to either activated or resting B cells (Fig. 4c and Supplementary Table 2,3). CD138^{hi} plasmablasts also exhibited 5-fold higher basal respiration compared to the other two populations analyzed (Fig. 4d). Notably, our RNA-seq data also showed that CD138^{hi} plasmablasts exhibit gene signatures consistent with induction of the unfolded protein response pathway that is induced upon plasma cell formation[26, 31] (Extended Data Fig. 4c and Supplementary Table 4), further supporting that blood-stage *Py* infection-induced CD138^{hi} plasmablasts are *bona fide* antibody secreting cells.

We next sought to investigate factors associated with the increased metabolism of CD138^{hi} plasmablasts. B cell activation and proliferation and increases in biomass require an ample supply of biomolecules such as N, S, PO_4 and C and the acquisition of amino acids, especially L-glutamine (L-glut) [32, 33]. This requirement raised the possibility that substantial numbers of CD138^{hi} plasmablasts triggered by blood-stage *Py* infection may deplete local metabolic resources in the spleen. In support of this hypothesis, targeted analysis of our RNA-seq data set revealed that multiple amino acid and nutrient transporters were differentially expressed among the splenic B cell populations (Fig. 4e and Supplementary Table 5). Ingenuity Pathway Analysis (IPA) revealed broad activation of genes encoding solute carrier (SLC) transporters that are involved in amino acid acquisition, particularly L-glut (Fig. 4f). The activation of these pathways was also associated with CD138^{hi} plasmablast metabolic hyperactivity and expression of Blimp-1, which is known to promote the expression of amino acid transporters[28]. We confirmed the upregulation of a set of L-glut SLCs, including mRNAs for *Slc1a4* and *Slc1a5*, which correlated positively with *Prdm1* and *Xbp-1* and inversely with *Pax5* mRNA expression (Fig. 4g). We also confirmed elevated mRNA and protein expression of *Slc7a5* (CD98), another key SLC transporter that mediates L-glut uptake[32, 33] (Fig. 4g–i). Together, these data support the hypothesis that metabolically hyperactive CD138^{hi} plasmablasts utilize SLC protein family members to increase the uptake of L-glut, which may in turn deplete key splenic metabolic resources required to sustain GC responses.

L-glutamine enhances anti-*Plasmodium* humoral immunity

Studies of *Plasmodium*-infected non-human primates and patients in malaria endemic areas revealed significant reductions in plasma L-glut concentrations during the acute phase of infection, which correlated with poorer outcomes and increased parasite burdens[34]. Similarly, splenic L-glut concentrations were reduced in *Py*-infected mice (Extended Data Fig. 5a). Given their numerical overrepresentation and increased expression of machinery required to uptake L-glut, we hypothesized that blood-stage *Py* infection-induced CD138^{hi} plasmablasts impede GC reactions by acting as a nutrient sink, effectively incapacitating GC B and/or T_{FH} cells. To test this hypothesis, we supplemented the drinking water of *Py*-infected mice with L-glut (H_2O+L-glut) and monitored parasite growth and various immune parameters. Notably, mice receiving *ad libitum* L-glut exhibited 65% lower total parasite burden compared to mice on regular drinking water (Fig. 5a,b). There were no observable impacts on parasite control when the drinking water was supplemented with either the essential branched chain amino acid L-alanine or the non-essential neutral amino acid L-valine (Extended Data Fig. 5b,c), which like L-glut is transported by SLC1A5. Importantly, the protective effects of L-glut supplementation required the presence of $CD4^+$ T cells (Fig. 5c), functional T_{FH} cells (Fig. 5d), and secreted antibody responses (Fig. 5e). Disruption of GC reactions via anti-CD40L also abrogated parasite control and GC B and T_{FH} cell responses in L-glut-treated mice (Extended Data Fig. 5d–f). Thus, enhanced parasite control in L-glut-treated mice was directly linked to improved GC reactions and humoral immunity, and not simply impacting upon the general physiology of either the host, host microbiome or the parasite itself.

Consistent with the requirements for secreted antibody and T_{FH} cells for enhanced parasite control following L-glut treatment, we observed higher magnitude GC B cell responses that appeared with accelerated kinetics (Fig. 5f and Extended Data Fig. 5g), as well as elevated numbers of class switched GC B cells in the spleen as early as day 12 p.i. (Extended Data Fig. 5h). While the numbers of $CD138^{hi}$ plasmablasts were not significantly affected (Extended Data Fig. 5i), L-glut supplementation also increased the numbers of GC-T_{FH}-like cells by day 12 p.i. (Fig. 5g and Extended Data Fig. 5j), but did not alter Bcl-6 expression within these cells (Extended Data Fig. 5k). The accelerated and enhanced GC B cell and T_{FH} cell responses also translated into higher serum titers of $MSP1_{19}$-specific IgG on both days 12 and 15 p.i. (Fig. 5h,i). Histological analyses confirmed L-glut treatment enhanced the retention of splenic/follicular architecture and elevated the number and size of GCs (Fig. 5j–l). L-glut supplementation did not enhance either T_H1-like cell responses or the activation status of splenic dendritic cells (Extended Data Fig. 5l,m), although these data do not formally exclude a potential role for their contribution to enhanced parasite control.

To investigate whether L-glut supplementation altered the metabolic status of splenic B cells, we sorted $CD138^{hi}$ plasmablasts and activated ($CD138^{lo}IgD^{neg}$) B cells, which includes both activated FO and MZ B cells, from spleens of *Py*-infected mice receiving either regular or L-glut supplemented water and measured oxygen consumption rates (OCR) (Fig. 5m). L-glut supplementation increased the basal OCR of activated B cells, but not $CD138^{hi}$ plasmablasts (Fig. 5n). Notably, L-glut could enhance parasite control when administered as late as day 6 p.i. (Extended Data Fig. 5n,o), but the protective effects were not observed when L-glut administration was initiated after the peak numerical expansion of plasmablasts (day 10 p.i.) (Extended Data Fig. 5p,q). Collectively, these data are consistent with the notion that $CD138^{hi}$ plasmablasts, by virtue of their metabolic hyperactivity and their potential to uptake L-glut, transiently impair the metabolic and optimal functions of other splenic B cell populations. Thus, L-glut, when delivered either prophylactically or therapeutically, may relieve GC B and T_{FH} cells from nutrient deprivation to enhance their numbers and functions.

Plasmablast deletion and L-glutamine are functionally redundant

The deletion of plasmablasts and L-glut treatment both reduce parasitemia, increase the GC response and boost the activation of B cells as measured by OCR. To test whether these phenotypes are connected, and determine whether $CD138^{hi}$ plasmablasts deletion and L-glut administration are functionally overlapping, we administered L-glut to DTx-treated CD138-DTR chimeric mice (Extended Data Fig. 6). As expected, both L-glut and DTx-treatment independently enhanced parasite control (Fig. 6a) and elevated the number of GC B cells (Fig. 6b) and GC-T_{FH}-like cells (Fig. 6c). However, these effects were not further enhanced when L-glut and DTx were combined (Fig. 6a–c). Furthermore, the metabolic activity of activated splenic B cells was elevated 8 to 12-fold in mice treated with either L-glut or DTx, yet the basal oxygen consumption was only minimally enhanced (~10%) when these treatments were combined (Fig. 6d). Taken together, these data suggest that $CD138^{hi}$ plasmablast deletion and L-glut supplementation are functionally redundant, which additionally supports the model that $CD138^{hi}$ plasmablasts may serve as a key glutamine sink during blood-stage *Plasmodium* infection.

Plasmablast deletion and L-glutamine improve immune memory

GC responses result in the production of LLPCs and MBCs that mediate protection against pathogen re-infection[5]. Accelerated and higher magnitude T_{FH} and GC reactions in DTx- and L-glut-treated mice are thus predicted to translate into increased numbers of MBCs, LLPCs and heightened resistance to a heterologous challenge with a lethal species of *Plasmodium* parasite, *P. berghei*-ANKA (*Pb*A). In support of this notion, kinetic analyses revealed higher frequencies and numbers of ($CCR6^+CD38^+$)[35] MBCs in both DTx- (Fig. 7a) and L-glut-treated (Fig. 7d) mice between days 10 and 60 p.i. DTx- and L-glut-treated mice also exhibited elevated LLPC responses, whether these were measured using functional ELISPOT assays (Fig. 7b,e) or flow cytometry (Extended Data Fig. 7a,b). Mice treated with either DTx (Fig. 7c) or L-glut (Fig. 7f) during a primary *Py* infection were also more resistant to lethal *Pb*A challenge, compared to their control counterparts. Of note, radiation chimeras are more resistant to lethal *PbA* challenge, which may explain the extended survival among both PBS- and DTx-treated chimeric mice, relative to the H_2O- and H_2O+L-glut-treated mice. Finally, we observed that MBC (Extended Data Fig. 7c) and LLPC (Extended Data Fig. 7d) responses were not enhanced when L-glut is adminstered from days 16–21 p.i., which is consistent with the therapeutic window during which L-glut functions to enhance parasite control (days 6–10 p.i.). Thus, the mechanisms by which L-glut promotes MBC and LLPC formation are likely linked to the enhanced function of the GC reaction and not strictly connected to enhancements in the post-GC survival of these cell subsets. Collectively, these data show that either $CD138^{hi}$ plasmablast deletion or therapeutic administration of L-glut during an established blood-stage *Plasmodium* infection can be sufficient to accelerate the formation and increase the magnitude of GC reactions, which are further associated with enhancements in MBC, LLPC and protective immune memory responses.

Robust plasmablast expansions during acute human malaria

To identify potential parallels between $CD138^{hi}$ plasmablast inductions in mice and plasmablast expansions during acute human malaria, we evaluated peripheral B cell responses in forty humans in *P. falciparum* blood-stage volunteer infection studies (VIS). Cohorts of malaria-naïve subjects were challenged with *P. falciparum* (*Pf*)-infected RBCs and blood parasite burdens were monitored by qPCR at regular intervals until the end of the study (EOS) on day 27–36 p.i. (Extended Data Fig. 8). Subjects were treated with a schizonticidal drug when the infection reached ~20,000 parasites/mL, at day 8 p.i. Importantly, acute blood-stage *P. falciparum* infection resulted in transient yet substantial increases in the frequencies of $CD19^+CD3^-CD27^+CD38^+$ plasmablasts by day 14/15 p.i, with some subjects exhibiting plasmablast responses that comprised greater than 15% of their entire peripheral B cell pool (Fig. 8a). Notably, the magnitude of plasmablast expansion was positively correlated with total parasite biomass (Fig. 8b). These clinical data show that plasmablast responses are robustly induced in malaria-naïve humans at their first exposure to *P. falciparum* in a way similar to experimental murine models of malaria.

Together, our observations in *P. falciparum*-infected humans, in combination with our rodent data, support the hypothesis that in malaria-naïve hosts the initial B cell activation events are numerically dominated by extrafollicular plasmablasts/$CD138^{hi}$ B cells. Futhermore, our

cellular, genetic and biochemical approaches support that plasmablasts functionally constrain germinal center responses and limit the induction of LLPC and MBC populations by acting as a metabolic sink that limits L-glut availability during experimental malaria.

Discussion

Rapidly forming, short-lived extrafollicular plasmablasts play complex roles in humoral immunity and host protection. Indeed, it is widely accepted that plasmablasts can provide an early source of protective antibody during bacterial infections[36, 37]. Similar to LLPCs, short-lived plasmablasts express Blimp-1 and are equipped with the machinery to secrete antibodies[1]. However, there are also data suggesting that plasmablasts may either inefficiently prime or directly inhibit T_{FH} cell activation and function[38, 39, 40], which may limit autoreactivity and tune the selection of B cell clones expressing the highest affinity receptors. While our data do not exclude the possibility that blood-stage *Plasmodium* infection-induced plasmablasts directly impair T_{FH} cell responses, our results show that either abrogation of plasmablast differentiation or deletion of plasmablasts during an established experimental *Plasmodium* infection resulted in enhanced clearance of the parasite, which was associated with 10-fold increases in the magnitude of the GC response. Our observations in mice are further supported by our *P. falciparum* VIS trials where substantial plasmablast expansions occured and were positively correlated with parasite burdens. Distinct from previous work showing immunosuppressive roles for either plasmablasts or plasma cells[38, 39] our data reveal $CD138^{hi}$ plasmablast populations comprise the dominant proportion of the total activated B cell pool following blood-stage *Plasmodium* infections. Thus, their overrepresentation may be a cardinal feature of blood-stage *Plasmodium* infections and potentially other infections of the blood that are associated with systemic inflammation, eryptosis, hemolysis, anemia and impairments in durable humoral immunity.

Plasmablast numbers have stood as a surrogate for protective immunity[41]. However, our assays revealed that few (~1%) plasmablasts express receptors that detectably interact with parasite antigens and that plasmablasts constrain rather than promote humoral immunity. Our efforts to identify potential mechanisms by which $CD138^{hi}$ plasmblasts constrain GC-dependent MBC and LLPC formation revealed links to their metabolism. From a cell biological perspective, *Plasmodium*-infection induced plasmablasts resemble a transient plasmablastic lymphoma similar to diffuse large B cell lymphoma (DLBCL) characterized by downregulation of tumor suppressor genes and upregulation of genes that promote tumorigenesis. Moreover, tumor cells[42, 43] and plasmablasts express an array of SLC molecules, likely to help meet the metabolic demands of their high rates of proliferation and increases in cellular biomass. It has also been reported that cancer cells are ‘addicted’ to glutamine and are capable of acting as a metabolic ‘sink’[44]. Thus, we hypothesized that the large numbers and increased metabolic demands of plasmablasts together with their high expression of SLC molecules may cause energetic and metabolic shortfalls for other effector B cells in the spleen, which may in turn functionally incapacitate and/or delay the development of GC response. Consistent with this hypothesis, our studies show that supplementing the drinking water of *Py*-infected mice with L-glut could relieve an apparent plasmablast-mediated state of nutrient deprivation and elevate GC, MBC and LLPC

responses. Our kinetic studies revealed a critical window during which L-glut supplementation can augment GC-dependent humoral immunity, which temporally overlaps with the expansion and maximal accumulation of *Plasmodium* blood-stage infection-induced plasmablasts. Thus, although both plasmablasts and GC B cells may exhibit similar metabolic requirements, the over-representation of plasmasblasts likely deprives GC B cells of critical nutrients required for their development and function. Future studies will be required to determine whether plasmablast deletion and associated changes in metabolic fitness of GC B cells also impact either B cell antigen receptor affinity maturation or epigenetic programming of MBCs and LLPCs. Although ^{13}C-L-glutamine tracing studies designed to show that plasmablasts sink glutamine *in vivo* are warranted, these studies are confounded by the time required for tissue processing and cell sorting. Nevertheless, the composite of data support the model that plasmablasts serve as a key glutamine sink during blood-stage *Plasmodium* infection and the hypothesis that alternative, metabolism-based strategies may have clinically relevant applications for malaria.

Previous studies reported that dietary supplementation of L-arginine enhanced T cell responses in rodents during lethal *Plasmodium* infection[45] and that inhibiting glutamine metabolism with 6-diazo-5-oxo-L-norleucine (DON) improved survival and prevented the onset of experimental cerebral malaria (ECM) in mice challenged with *Pb*-ANKA[46]. No mechanisms were identified in the L-arg study and the latter report primarily attributed the effects of DON to inhibition of $CD8^+$ T cell degranulation, a key function that drives the onset of ECM. During experimental *Plasmodium yoelii* and *Pb*-ANKA infections truncated with anti-blood-stage drugs, neither of which cause $CD8^+$ T cell-mediated immunopathology and ECM, $CD8^+$ T cells were robustly activated[22] and contribute to host protection[47]. Thus, our data do not exclude the possibility that an enhanced parasite-specific CD8 T cell response also contributes to the improvements in host resistance to *Plasmodium* during L-glut supplementation. We predict that strategies to specifically inhibit L-glut uptake by plasmablasts would yield results similar to those we observed when we either abrogated plasmablast development or deleted these cells using genetic approaches. However, at present we know of no way to block either glutamine uptake or glutaminolysis specifically in plasmablasts. Nevertheless, our data and the experiments with L-arg and DON during experimental malaria highlight critical roles for immune cell metabolism and warrant the further exploration of strategies to modulate these cell biological processes in specific cell types.

In summary, our data support the model that during blood-stage *Plasmodium* infection, B cell differentiation is biased towards metabolically hyperactive, short-lived plasmablast responses that by their sheer numbers constrain GC reactions, likely due to glutamine deprivation. The preferential induction of extrafollicular, immunosuppressive plasmablasts represents an additional mechanism by which *Plasmodium* parasites subvert host protective immunity. Thus, the identification of an expansion of immuno-inhibitory plasmablasts during *Plasmodium* infection represents a conceptual shift with implications for either future immune- or metabolism-based strategies designed to limit plasmablast expansions, which may ultimately contribute to the development of durable humoral immunity against malaria.

Methods

Volunteer infection studies

P. falciparum blood-stage Volunteer infection trials (VIS), inoculum preparation, volunteer recruitment, infection, monitoring and treatment were performed as previously described[48]. In brief, healthy malaria-naive individuals (n = 36 men, n = 4 women) underwent induced blood-stage malaria inoculation with 2800 viable *P. falciparum* 3D7-parasitized RBCs, and peripheral parasitemia was measured at least daily by qPCR as described previously[49]. Participants were treated with antimalarial drugs at day 8 of infection. Blood samples from 40 volunteers (from 4 studies across 6 independent cohorts) were collected prior to infection (day 0), at peak infection (day 8) and 14 or 15 and 27–36 days (end of study, EOS) after inoculation (in analyses these time points are grouped as 0, 8, 14/15 and EOS). Plasma was collected from lithium heparin whole-blood samples according to standard procedures, snap frozen in dry ice and stored at −70°C. B-cells were analyzed from fresh whole blood at time of collection. All studies were registered with US NIH ClinicalTrails.gov (NCT02867059, NCT02783833, NCT02431637[50], NCT02431650[50]). Participants were healthy adults 18 and 55 years with no prior exposure to malaria or residence in malaria-endemic regions. Area under the curve (AUC) were calculated using the trapezoidal method on serial $\log_{10}$ transformed parasites/mL data from 4 days p.i. to each of the three defined timepoints (8, 14/15, and EOS similar to previously described[51]. Equation 1 below describes the calculation, with being each time point sampled, being the $\log_{10}$ parasites/mL at that time, and being either 8 p.i., 14/15 p.i., or EOS. Samples where parasitaemia was not detected were substituted with 0 on the $\log_{10}$ scale. The samples collected between the 4 defined timepoints (ranging from daily to twice daily before treatment, ranging from daily to every 2 h after treatment, and ranging from every four days to daily between timepoint 14/15 and EOS) were used in the calculation of AUC but not in any other analyses.

Study approval

Written informed consent was obtained from all participants. Ethics approval for VIS and the use of human samples was obtained from the Human Research and Ethics Committee of the QIMR-Berghofer Institute of Medical Research and Alfred Human Research and Ethics Committee for the Burnet Institute.

Animals, infections and parasitemia quantification

The University of Iowa IACUC approved all experiments. C57BL/6 WT (CD45.2 and CD45.1), Blimp-1eYFP (JAX stock #008828), μMT (JAX stock 002288) and *Rosa26-ERT2/Cre* (JAX stock 008463) mice were purchased from Jackson Laboratories. *Aicda*$^{-/-}$μs$^{-/-}$ mice were a gift from F. Lund (UAB). CD138-DTR mice were generated via CRISPR/Cas9 editing at the U of Iowa genome editing facility. Male and female mice were used in all experiments, sex-matched only for adoptive transfers and generating chimeras. *Plasmodium yoelli* (clone 17XNL, obtained from MR4, ATCC) and *Plasmodium berghei* (clone ANKA, obtained from MR4, ATCC) stocks were generated by single passage in NIH Swiss Webster mice. Infections in experimental mice were initiated by a serial transfer (i.v.) of 1×10^6 parasitized red blood cells (pRBCs) derived from a single donor C57BL/6 mouse. In some experiments, *Py*-infected mice were treated (i.p.) daily (days 8–11 p.i.) with 500 μg of either

anti-CD40L (clone MR1) or Armenian Hamster IgG. CD4 T cell depletion was achieved by administering (i.p.) 200 μg of anti-CD4 antibody (clone GK1.5, BioXcell) on days 5 and 7 p.i. Parasitemia was measured using flow cytometry and is also depicted as area under the curve (AUC), which is a composition of parasite growth, peak burden and clearance kinetics[5253].

CD138^{hi} adoptive transfers

Splenic CD138^{hi} B cells were enriched on day 5 p.i. using anti-CD138-APC (clone 281–2, BioLegend) and anti-APC magnetic beads (Miltenyi). CD19^{+}CD138^{hi}IgD^{neg} plasmablasts and CD19^{+}CD138^{lo}IgD^{neg} activated B cells were sort purified. 1–2 × 10^{6} cells were transferred i.v. to mice on day 7 p.i. Mice that did not receive cells were given 200 μL of PBS i.v. on day 7. Sera and spleens were harvested from recipients on day 21 p.i. (day 14 post-transfer). Parasitemia was monitored every 2–3 days p.i.

Electron Microscopy

Electron microscopy was performed by the Central Microscopy Research Facility personnel at the University of Iowa. Images were captured on JEOL JEM 1230.

Confocal Imaging

After harvest, spleens were passed through a sucrose gradient (10% for 1 h, 20% for 2 h, 30% for 3 h) and flash frozen in Tissue Freezing Medium (General Data TFM-5) using a Gentle Jane Snap Freezer. 10 μm sections were cut and dried for 45 min in a 37 °C dry incubator. The sections were soaked in ice-cold Zinc Formalin Fixative (Sigma) for 15 min at −20°C then washed in 1× PBS (3 min/ wash). Sections were blocked with 1% BSA in 1× PBS for 2 h at 25 °C. After a 5-min wash in 1× PBS, sections were stained with the primary antibodies (in 1% BSA in 1× PBS) for 24 h at 4 °C. Sections were washed in 1× PBS (3 min/ wash) then mounted using hard set mounting medium for fluorescence (VECTASHIELD H-1400). Sections were stained with B220-AF488 (5 μg/ml; clone RA3–6B2, eBioscience), CD4-AF594 (10 μg/ml; clone GK1.5, BioLegend). GL7-AF647 (6.67 μg/ml; BD Pharmingen), and CD138-BV421 (1.67 μg/ml; clone 281–2, BioLegend). Imaging was done using a Zeiss LSM710 confocal microscope and processed using IMARIS x64 software (version 9.2.1).

Bone marrow chimeras

For generation of *Rosa26-ERT2/Cre Prdm1*$^{fl/fl}$: μMT chimeras, WT recipient (CD45.1) mice were irradiated with 475 rads twice separated by 4 h. Bone marrow cells from *Rosa26-ERT2/Cre Prdm1*$^{fl/fl}$ (CD45.2) and μMT (CD45.1) were mixed 1:9 and 1 × 10^{7} cells were injected i.v. Mice were maintained on Uniprim diet (Envigo) for 2–3 weeks. Chimerism was assessed at 6 weeks and mice were infected with 10^{6} *Py* parasitized RBCs by 8 weeks. On days 5 and 7 post infection mice were either treated orally using a gavage needle, with 100 μL tamoxifen (4 mg/mouse) or corn oil. Depletion of plasmablasts was assessed on day 10.

For generation of CD138-DTR chimeras, WT (CD45.2) mice were irradiated with 475 rads twice separated by 4 h. 1 × 10^{7} cells bone marrow cells from CD138-DTR mice were injected i.v. Mice were maintained on Uniprim diet (Envigo) for 2–3 weeks. Chimerism was

assessed at 6 weeks and mice were infected with 10^6 *Py* parasitized RBCs. On days 5 and 7 post infection mice were treated i.p. with either diphtheria toxin or PBS intraperitonially. Depletion of plasmablasts was confirmed on day 10 p.i. For *Rosa26-ERT2/Cre Prdm1*$^{fl/fl}$: μMT : WT chimeras, bone marrow cells from *Rosa26-ERT2/Cre Prdm1*$^{fl/fl}$ (CD45.2), μMT (CD45.1), WT (CD45.1) were mixed at 1:8:1 and 10^7 cells were injected i.v into *Rag1*$^{-/-}$ mice irradiated with 475 rads. Mice were maintained on Uniprim diet as above. Chimerism assessements, infections and tamoxifen treatments were as described above.

Tamoxifen and diphtheria toxin preparation and treatment

1 g of dessicated Tamoxifen (Sigma T5648) was dissolved in 5 mL of 200 proof ethanol, mixed with 20 mL of corn oil and stored at −20°C. On days 4, 5, and 6 post *Py* infection mice were administered 100 μL (4 mg/ mouse/dose) of the Tamoxifen corn oil mixture via oral gavage. 1 mg of lyophilized DTx (Sigma D0564) was resuspended in 3 mL of sterile PBS to achieve a concentration of 0.33 mg/mL. Mice were treated i.p. with 250 ng of DTx on the indicated days.

RNA Seq and GSEA

The three different B cell populations (resting B cells, activated B cells and plasmablasts) were flow-sorted from 4 *Py*-infected mice on day 10 p.i and RNA was extracted using NucleoSpin RNA kit (Takara Bio USA Inc.) according the manufacturer's protocol. RNA sample integrity and quantity were determined using Tape Station Bioanalyzer (Agilent), with all samples showing RNA integrity numbers > 8. Twenty ng of total RNA was used for each library. Strand-specific RNA-Seq library was created using Illumina library creation protocol. The indexed libraries were pooled and sequenced using an Illumina NextSeq 550 sequencer using paired-end chemistry with 50 base pair (bp) read length Gene Expression Omnibus record: GSE134548. The quality of sequence reads was assessed using FastQC (http://www.bioinformatics.babraham.ac.uk/projects/fastqc/) and were aligned using STAR aligner[54] to the mouse genome version mm10 and the corresponding transcriptome. Following read alignment, gene expression profiles were computed using featureCounts[55]. Next, differentially expressed genes were identified using Partek GS software and genes with significant changes were filtered using adjusted *P*-value of 0.05 as threshold. Visualization of differentially expressed genes represented as heat maps were generated using Partek GS software. Further, Ingenuity Pathway Analysis software (Qiagen Bioinformatics) was used to identify the underlying molecular pathways and interaction networks that involved the differentially expressed genes.

Quantitative Real Time PCR and Primers

The three different B cell populations (resting B cells, activated B cells and plasmablasts) were flow-sorted from 4 *Py*-infected mice on day 10 p.i. and RNA was extracted using NucleoSpin RNA kit (Takara Bio USA Inc.) according the manufacturer's protocol. Two micrograms of RNA was used for cDNA synthesis. One microliter cDNA was added to 19 μL of PCR mixture containing 2X PowerUp SYBR Green Master Mix and 0.2 μM of forward or reverse primers. Amplification was performed in a QuantStudio3 thermocycler (Appiled Biosystems). Genes and forward and reverse primers are shown in Supplementary Table 6. Cycle threshold (*Ct*) values were normalized to those of the housekeeping gene

hypoxanthine phosphoribosyltranferase (*Hprt*) by the following equation: $\Delta Ct = Ct_{(\text{gene of interest})} - Ct_{(\text{HPRT})}$. All results are shown as a ration of HPRT calculated as $2^{-(\Delta Ct)}$.

ELISPOT

White polystyrene plates (Nunc Maxisorp) were coated with 0.5 μg/ml of either recombinant $MSP1_{19}$ or parasite infected red blood cell lysate. Plates were washed with PBS and blocked for at least 2 h with PBS/2.5% BSA/5% Goat Serum. Bone marrow cells or $CD19^{+}CD138^{+}IgD^{neg}$ B cells sort-purified from *Py*-infected mice were used. Serial dilutions of cells in supplemented IMDM were added to each well for 20 h at 37 °C with 5% CO_2. Following extensive washes with PBS/0.05% Tween 20, HRP-conjugated goat anti-mouse IgM and IgG was added overnight at 4°C. Spots were developed with 3-amino-9-ethylcarbazole.

Metabolic flux analysis

Flow-sorted B cell populations (resting B cells, activated B cells and plasmablasts) from at least 3 *Py*-infected (day 10 p.i.) were plated at 250,000 cells per well in poly-lysine coated Seahorse XF96 cell culture microplate. Cells were allowed to adhere for 30 min to 1 h. OCR was measured in modified DMEM containing 2 mM L-glutamine (XF media) under basal conditions in a 96-well extracellular flux assay using a Xfe-96 (Seahorse Bioscience). In experiments comparing metabolic activity of B cell populations sorted from mice maintained on either regular water or water supplemented with L-glutamine, the culture medium was devoid of L-glutamine.

Metabolite measurements

Frozen spleens from naïve and Py-infected mice (~40 mg) were lyophilized, extracted and analyzed as described previously[56]. Briefly, gas chromatography/mass spectrometry were utilized for biochemical detection of metabolites by automated comparison of ion features in samples to a reference library of chemical standards entries, including retention time, molecular weight (m/z), preferred adducts, and in-source fragments as well as associated MS spectra.

Amino acid supplementation

Drinking water of Py-infected mice was supplemented (2.8 g/dL) with either L-glutamine, L-valine or L-alanine (Sigma Aldrich) starting at the indicated timepoints.

ELISA

Plates (Nunc Maxisorp) were coated either with 0.5 μg/mL $MSP1_{19}$ (MR4) or 18 μg/mL total parasite lysate and blocked with 2.5% BSA + 5% normal goat serum. After washing wells with ELISA wash buffer (PBS+ 0.05% Tween 20; 250 μL/ well, 3 min/wash), serially diluted serum samples from naïve and *Py*-infected mice were added and incubated for 18 h at 4 °C. Plates were washed and $MSP1_{19}$-specific or parasite specific antibodies were detected with HRP-conjugated goat anti-mouse IgG or IgG1 or IgG2b (in ELISA blocking buffer). After washing, plates were developed with SureBlue reserve TMB Kit (KPL) according to the manufacturer's protocol and absorbance was at OD_{450} using a Spectra Max

340 (Molecular Devices). End point titers were extrapolated from sigmoidal 4PL (where X is log concentration) standard curve for each sample. The threshold for end point titers is the mean plus 4–8× s.d. recored for naïve mouse sera.

For ex vivo $CD138^{hi}IgD^{neg}$ B cell ELISA, 8×10^4 $CD19^{+}CD138^{hi}IgD^{neg}$ plasmablasts were sort purified from day 10 p.i. mice and cultured in supplemented IMDM (10% FBS, 2 μM glutamine, 100 U/mL penicillin, 100 μg/mL streptomycin, 50 mM β-mercaptoethanol) in the presence of 5 ng/ml *P. yoelii* parasite lysates. Supernatants were recovered after 3 days of culture. $CD138^{hi}$ B cell supernatants were diluted 1:2 and added to previously blocked total parasite lysate coated Nunc plates and processed as described above.

Cell staining and Flow cytometry

For cellular analyses of splenic cells, mouse spleens were forced through a 70 μm mesh to generate single-cell suspensions. The single-cell suspension of splenocytes were subjected to red blood cells lysis, were counted and resuspended at 10^6 cells/100 μL. Fc receptors were blocked using Fc block/CD16/32 (clone 2.4G2) in FACS buffer (PBS+0.09% Sodium Azide +2% FCS) for 15 min at 4 °C followed by cell specific staining protocols as described below. For detecting GC-T_{FH}-like cells, cells were stained with purified rat α mouse CXCR5 (1:100; clone 2G8, BD Biosciences) in T_{FH} staining buffer (PBS+0.09% Sodium Azide +2% FCS+0.5%BSA+2% mouse serum) for 1 h at 4 °C. Cell were washed in FACS buffer, spun at 300 × g for 5 min at 4 °C and resuspended in Biotin SP-conjugated Affinipure Goat-anti-rat IgG (H+L) F(ab) (1:1000, Jackson Immunoresearch) in T_{FH} staining buffer and incubated for 30 min at 4 °C. Cell were washed in FACS buffer, spun at 300 × g for 5 min at 4 °C and resuspended in an antibody cocktail containing CD4-PercP Cy5.5 (1:300; clone GK1.5; BioLegend), CD44-AF700 (1:1000; clone IM7; BioLegend), CD11a-FITC (1:300; clone M17/4; BD Biosciences), PD-1-PE or PE-Cy7 (1:300; clone RMP1–14; BioLegend) and streptavidin-BV421 (1:500) and incubated 30 min at 4 °C. The cells were washed with FACS buffer as before and resuspended in FACS buffer before acquisition. For B cell staining, cell were stained with rat anti-mouse B220-PercP-Cy5.5 (1:300; clone RA3–6B2; BioLegend), rat anti-mouse CD19-AF700 or PE (1:300; clone 6D5; BioLegend), rat anti-mouse IgD-Pac Blue or BV510 (1:500; clone 11–26c.2a; BioLegend), rat anti-mouse CD138-APC or Pac Blue (1:250; clone 281–1; BioLegend) (for plasmablast staining); rat anti-mouse GL7-PE (1:300; BioLegend) and hamster anti mouse CD95-FiTC (1:300; clone Jo2; BD Biosciences) (for GC B cell staining); rat anti mouse CD23-PE Cy7 (1:300; clone B3B4; BioLegend) and rat anti-mouse CD21-APC (1:300; clone 7E9 BioLegend) (for marginal zone B cell staining). For human B cell staining, 200 μl of blood was stained with surface antibodies to CD19 (FITC, clone HIB19), CD27 (AF700, clone M-T271) CD38 (BV785, clone HIT2).

BrdU and FLICA Staining

BrdU (Sigma) was injected i.p. at 2 mg and supplemented in the drinking water at 0.8 mg/ml from days 6–10 p.i. FLICA reagent was prepared and added to cells according to manufacturer's instructions (Thermofisher). For BrdU staining, cells were permeabilized, treated with 3 μg/mL DNAse (Invitrogen) and subjected to intracellular staining with either anti-BrdU-FITC (clone PRB-1) or mouse IgG1-FITC.

Statistical Analysis

Statistical analyses, end point titers, and overall parasite burden, represented as area under the curve for rodent studies were performed using GraphPad Prism 6 software (GraphPad). Specific tests of statistical significance are detailed in the figure legends.

Data Availability Statement

The data that support the findings of this study are available as Source Data files and from Gene Expression Omnibus GSE134548. All data are available from the corresponding author upon request.

Extended Data

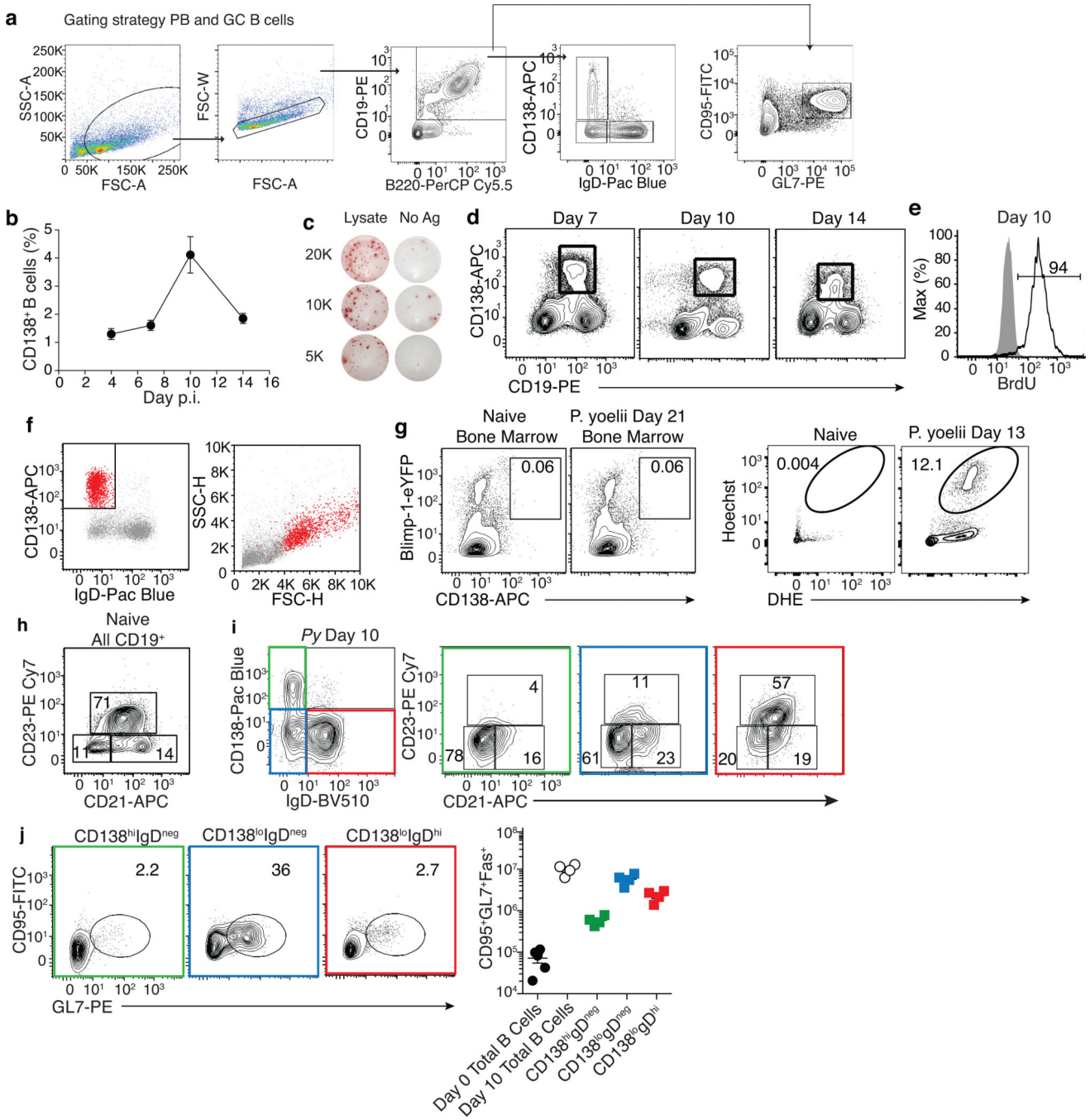

Extended Data Fig. 1. Experimental malaria expands extrafollicular plasmablast populations

a, Gating strategy for identifying plasmablasts ($CD138^{hi}IgD^{neg}$), activated ($CD138^{lo}IgD^{neg}$) and resting B cells ($CD138^{lo}IgD^{hi}$). **b**, kinetics of PB in blood. Data are means ± s.d, representative of $n = 2$ biologically independent experiments with similar results using $n = 3$ mice/time point. **c**, $CD138^{hi}IgD^{neg}$ plasmablasts were sort-purified from *Py*-infected mice on day 10 p.i., cultured for 20 hours and parasite lysate-specific IgM and IgG secreting ASCs were detected. Representative wells of ELISPOT assay. **d**, Relative CD19 expression by $CD138^{hi}IgD^{neg}$ plasmablasts on days 7, 10, and 14 post *Py* infection. Data are

representative of $n > 5$ experiments with similar results. **e**, BrdU incorporation in $CD138^{hi}IgD^{neg}$ plasmablasts was assessed on day 10 p.i. Histogram represents BrdU staining, solid gray histogram is isotype (mouse IgG1). Data are representative of $n = 2$ experiments with similar results using $n = 8$ mice. **f**, Forward scatter and side scatter of $CD138^{hi}IgD^{neg}$ plasmablasts examined on day 10 p.i. Data are representative of $n > 5$ experiments with similar results. **g**, Blimp-1/eYFP reporter mice were infected with Py. $CD138^{hi}$ Blimp-1/$eYFP^{+}$ cells in bone marrow from naïve (left panel) or day 21 infected mice (right panel). Data are representative of $n = 2$ independent experiments with similar results using $n = 4$ mice/group. **h**,**i**, CD21 and CD23 expression by B cells in a naïve mouse (**h**) and day 10 Py-infected mouse (**i**) showing plasmablasts (green box) activated (blue box) and resting (red box) B cells. Data are representative of $n > 5$ experiments with similar results using $n = 3$ mice/group. **j**, Representative plots of the frequency and total numbers of GC B cells ($GL7^{+}CD95^{+}$) among plasmablasts, activated and resting B cell populations on day 10 p.i. Data are means ± s.e.m., representative of $n = 3$ experiments with similar results using $n = 5$ (Day 0 Total B cells) and $n = 4$ mice (each remaining group).

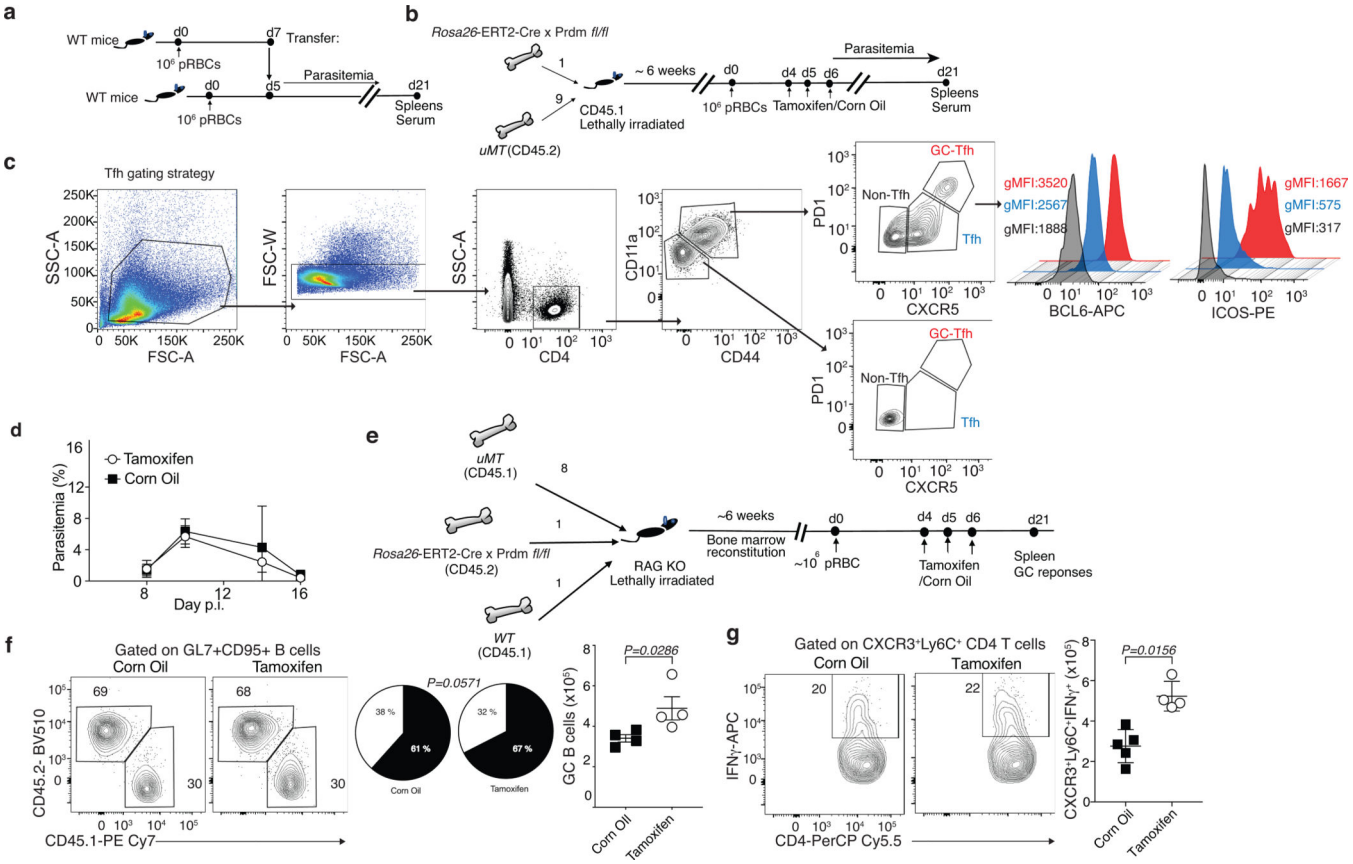

Extended Data Fig. 2. Developmental abrogation of blood stage *Plasmodium* infection-induced plasmablast responses.

a, Experimental design for adoptive transfers. **b**, Experimental design for Rosa26-ERT2/Cre × Prdm1$^{fl/fl}$ (CD45.2) : µMT bone marrow chimeric system. Eight weeks after engraftment, mice were infected with 1 × 10^6 *Py* and then treated with either corn oil or tamoxifen on days 4, 5, and 6 p.i. **c**, Gating strategy of T_{FH} cells. **d**, Kinetics of parasite burden in *Py*-infected wild-type mice treated with tamoxifen or corn oil on days 4, 5, and 6 p.i. Data are means ± s.e.m., pooled from $n = 2$ biologically independent experiments with $n = 6$ mice/group. **e**, Experimental design for the three-way mixed bone marrow chimera. **f**, Eight weeks after engraftment, mice were infected with *Py*, treated with either corn oil or tamoxifen on days 4, 5, and 6 p.i. and the relative proportions (pie diagram) of *Prdm1*$^{fl/fl}$ (CD45.2) and wild-type (CD45.1) cells in the GC B cell compartment was analyzed. Data are means ± s.e.m., pooled from $n = 2$ biologically independent experiments with $n = 4$ mice/group. **g**, Evaluation of T_H1 responses in PBS and tamoxifen-treated mixed bone marrow chimeric mice (as shown in b). Data are means ± s.d. representative of $n = 2$ biologically independent experiments with similar results using $n = 5$ (corn oil) and $n = 4$ mice (tamoxifen). Data in f,g were analyzed using two-tailed Mann-Whitney. Symbols and symbols represent individual mice.

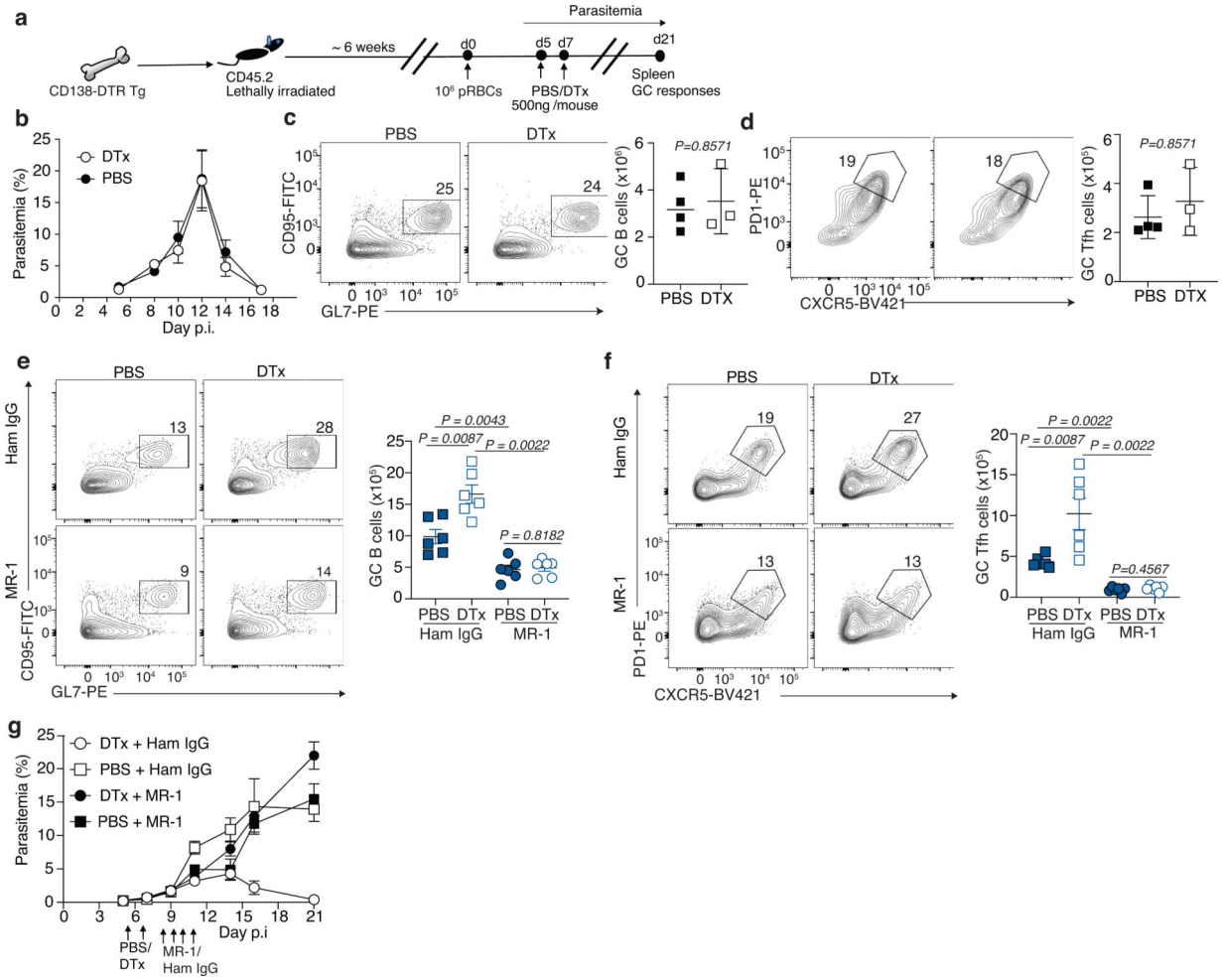

Extended Data Fig. 3. Deletion of blood stage *Plasmodium* infection-induced plasmablast responses

a, Experimental design for generating CD138-DTR chimeras. Eight weeks after engraftment, mice were infected with 1×10^6 *Py* and on days 5 and 7 p.i. treated with either DTx or PBS to delete plasmablasts. Data are means ± s.d., representative of $n = 2$ independent experiments with similar results using $n = 4$ mice/group. **b**-**d**, *Py*-infected wild-type mice were treated with either DTx or PBS on days 5 and 7 p.i. Kinetics of parasite burden (**b**), representative plots and summary data of GC B cells (**c**) and GC-Tfh cells (**d**) on 21 p.i. Data are means ± s.d., representative of $n = 2$ biologically independent experiments with similar results using $n = 4$ (PBS) and $n = 3$ mice (DTx). **e**-**g**, CD138-DTR chimeric mice were infected with 1×10^6 *Py*, plasmablasts were deleted with DTx and mice were subsequently treated with either MR-1 (anti-CD40L) or hamster IgG on days 8–11 p.i. Representative plots and summary data of GC B (**e**) and GC-TFH (**f**) cells as measured on day 21 p.i. and kinetics of parasite burden (**g**). Data are means ± s.e.m., pooled from $n = 2$ biologically independent experiments with $n = 6$ mice/group. Symbols in c-f represent individual mice and data were analyzed using two-tailed Mann-Whitney.

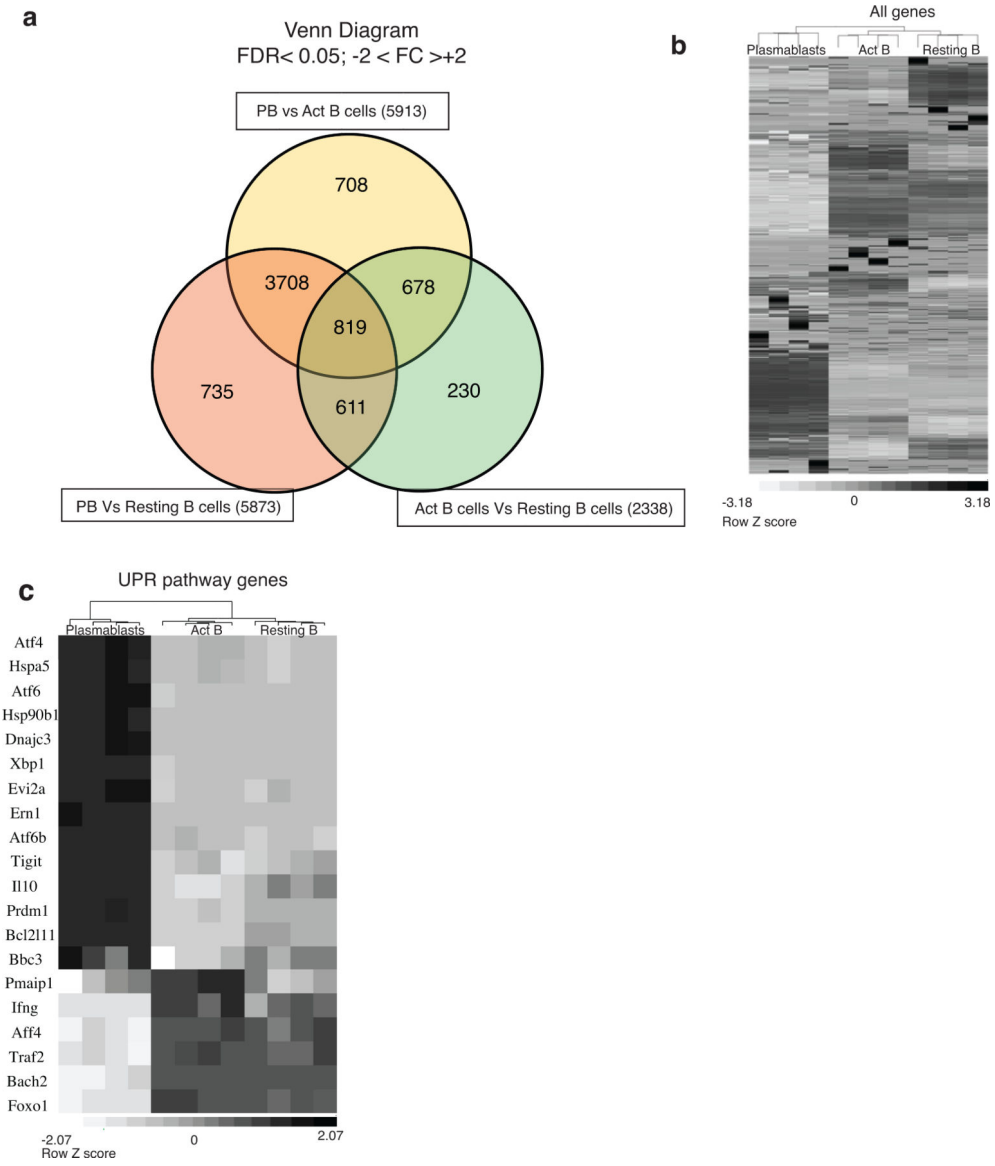

Extended Data Fig. 4. Differentially expressed genes among splenic B cell populations

a, Venn diagram showing differentially expressed genes assessed by RNA-seq among the three splenic B cell populations on day 10 p.i. Respective cell types were sort-purified from $n = 4$ *Py*-infected mice. Data were obtained from one RNA-Seq experiment. Two-tailed ANOVA was used for identifying differentially expressed genes. **b**, Heat map showing the relative expression of all annotated genes assessed using RNA-Seq. **c**, Heat map showing the relative expression of genes involved in the unfolded protein response pathway (UPR).

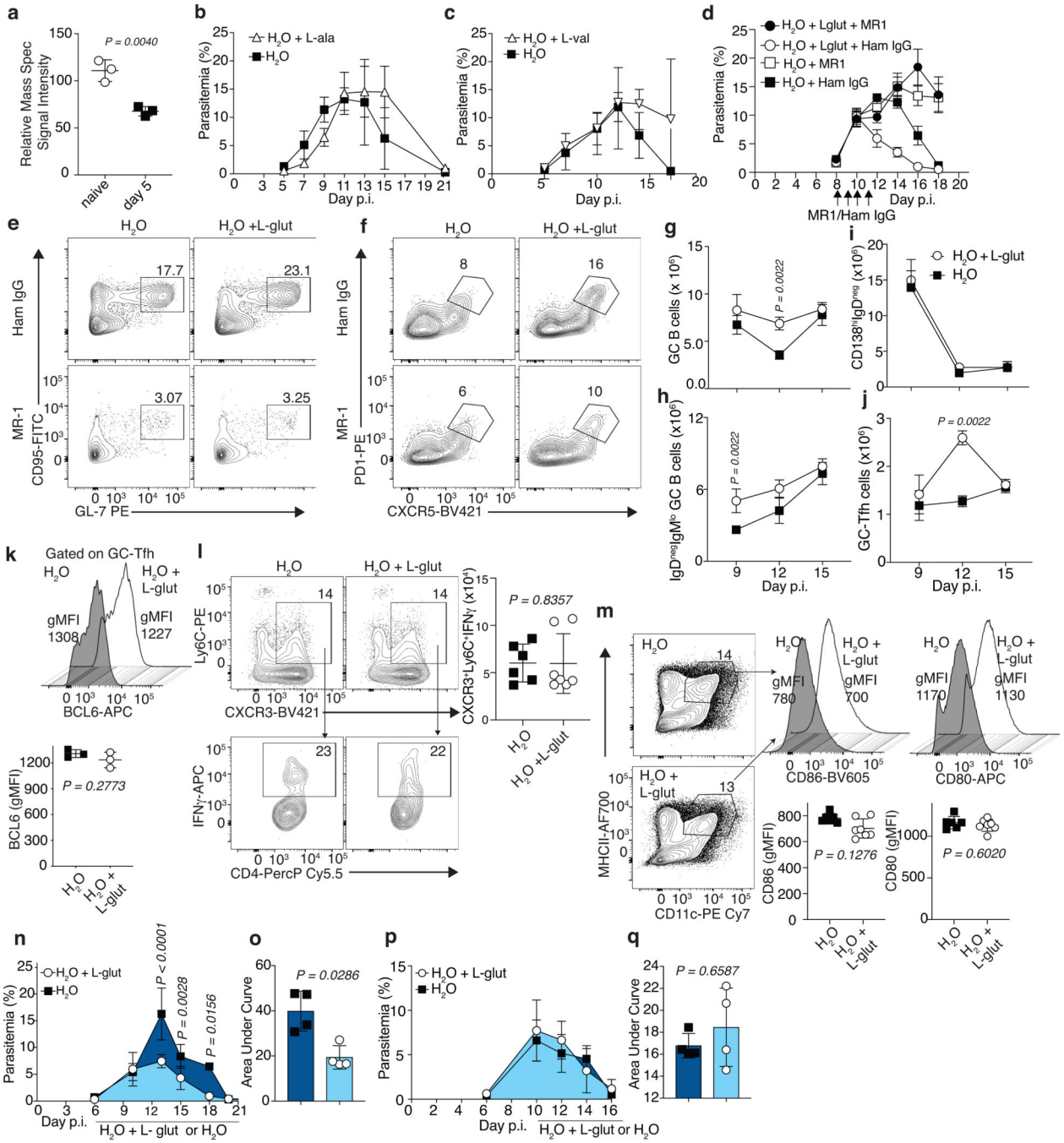

Extended Data Fig. 5. L-glutamine enhances GC responses during experimental malaria

a, L-glut concentrations in the spleens of naive and Py-infected wild-type mice on day 5 p.i. Data are means ± s.d. representative of $n = 2$ biologically independent experiments with similar results using $n = 3$ mice/group analyzed by a two-tailed unpaired t test (DF = 4; t = 5.933). **b**,**c**, Kinetics of parasite burden in mice treated with either L-alanine (**b**, H_2O + L-ala), L-valine (**c**, H_2O + L-val) or water starting on day 0 p.i. Data are means ± s.d., representative of $n = 2$ independent experiments with similar results using $n = 3$ mice/group. **d-f**, Py-infected wild-type mice were treated with L-glutamine (H_2O + L-glut) or water

starting day 0 p.i. and subsequently treated with MR-1 (anti-CD40L) or Hamster IgG antibody on days 8–11 p.i. Kinetics of parasite burden (**d**) and frequency of GC B cells (**e**) and GC-Tfh cells (**f**) on day 21 p.i. Data in d are means ± s.e.m, pooled from $n = 2$ independent experiments with $n = 7$ mice/group. Data in e,f are representative of $n = 2$ biologically independent experiments with similar results using $n = 3$ mice/group. **g-m**, Py-infected wild-type mice were treated with L-glutamine (H_2O + L-glut) or water starting day 0 p.i. Kinetics of GC B cells (**g**), class-switched GC B cells (**h**), plasmablasts (**i**), and GC-T_{FH}-like cells (**j**). Data in g-j are means ± s.d., representative of $n = 2$ biologically independent experiments with similar results using n = 6 mice/group analyzed by two-tailed Mann-Whitney. **k**, gMFI of BCL6 on GC-T_{FH}-like cells. Data are means ± s.d., representative of $n = 2$ biologically independent experiments with similar results using $n = 3$ mice/group analyzed by two tailed unpaired t test (DF = 4; $t = 1.257$). Number of T_H1 cells (**l**, Ly6C+CXCR3+IFNg+) and gMFI of CD80 and CD86 expression on splenic dendritic cells (**m**, MHCII+CD11c+) on day 10 p.i. Data in l,m are means ± s.e.m, pooled from $n = 2$ biologically independent experiments with $n = 6$ (H_2O) and $n = 7$ mice (H_2O + L-glut) analyzed by two-tailed Mann-Whitney. **n**,**o**, Kinetics of parasite burden (**n**) and area under curve as a measure of total parasite biomass (**o**) in Py-infected wild-type mice treated with L-glutamine (H_2O + L-glut) starting on day 6 p.i. Data in n are means ± s.d., representative of $n = 2$ biologically independent experiments with similar results using $n = 4$ mice/group. Data in n analyzed using two-way ANOVA with Sidak's multiple comparison (DF = 5; F = 5.728). Data in o analyzed with two-tailed Mann Whitney. **p**,**q**, Kinetics of parasite burden (**p**) and area under curve (**q**) as a measure of total parasite biomass in Py-infected wild-type mice treated with L-glutamine (H_2O + L-glut) starting day on 10 p.i. Data in p,q are means ± s.d., representative of $n = 2$ independent experiments with similar results using $n = 4$ mice/group analyzed by two-tailed Mann Whitney. Symbols in a, l-q represent individual mice.

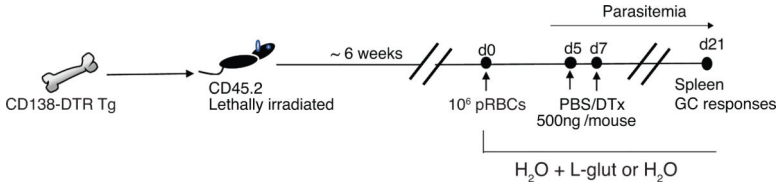

Extended Data Fig. 6. Experimental design for treating CD138-DTR: WT chimeras with L-glutamine

Eight weeks after engraftment, mice were infected with Py and treated with L-glut or water starting on day 0 p.i. Mice were subsequently treated with either DTx or PBS on days 5 and 7 p.i. to delete plasmablasts.

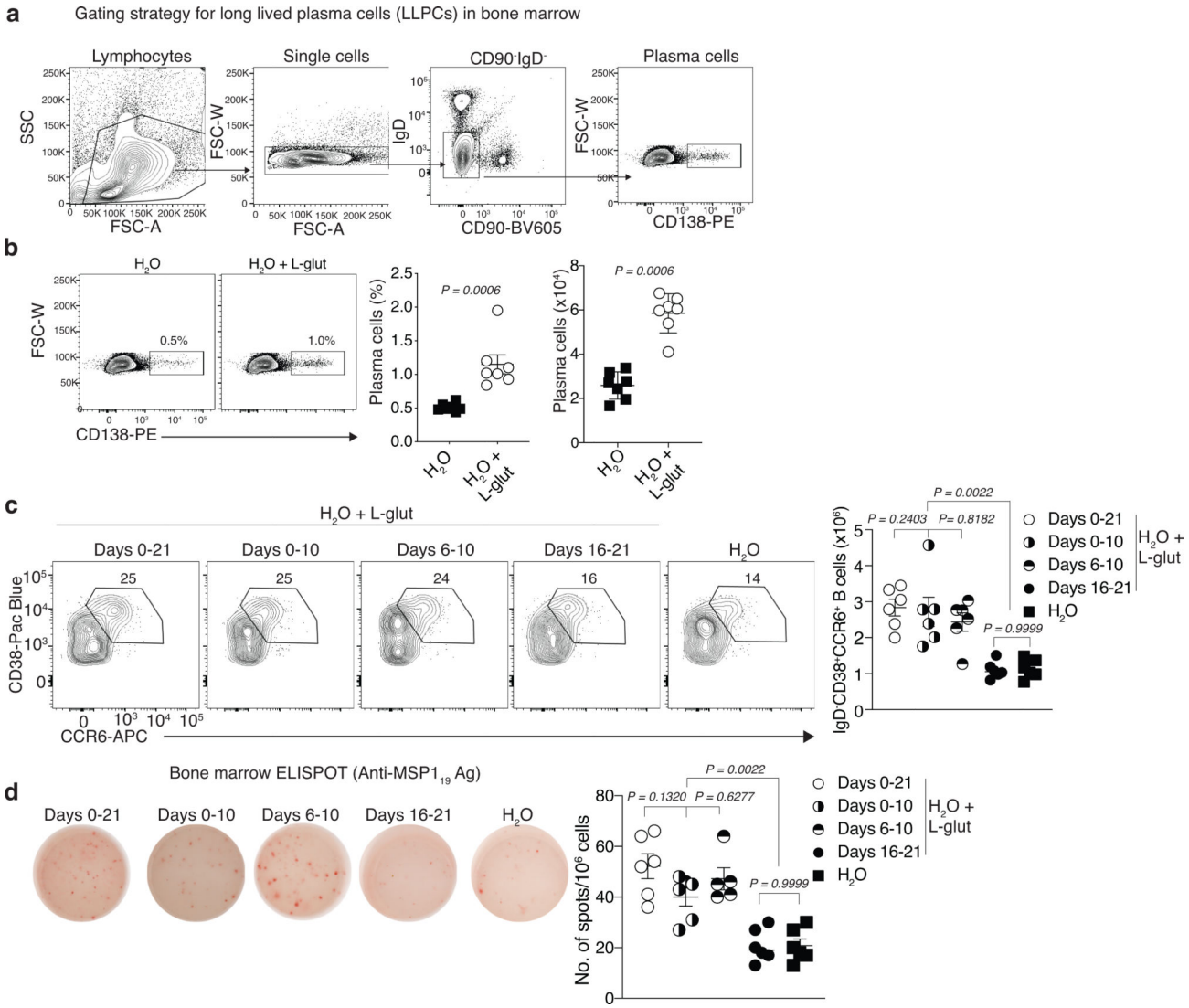

Extended Data Fig. 7. Post-GC administration of L-glutamine does not appreciably enhance LLPC and MBC responses

a, Gating strategy for long lived plasma cells (LLPCs) in the bone marrow of Py-infected mice. **b**, Numbers of LLPCs in the bone marrow on day 60 p.i. from Py-infected mice treated with either L-glutamine (H_2O + L-glut) or water (H_2O). Data are means ± s.e.m., pooled from $n = 2$ biologically independent experiments with $n = 7$ mice/group analyzed by two-tailed Mann Whitney. **c**,**d**, Py-infected wild-type mice were treated with either L-glutamine (H_2O + L-glut) or water (H_2O) at indicated time points p.i. and analyzed on day 30 p.i. Numbers of splenic memory B cells (**c**, CCR6+CD38+) and representative ELISPOT wells and summary data (**d**) demonstrating number of antibody-secreting LLPCs in the bone marrow. Data in **c**,**d** are means ± s.e.m, pooled from $n = 2$ biologically independent experiments with $n = 5$ (d, days 6–10) and $n = 6$ mice (remaining groups) analyzed by two-tailed Mann Whitney. Symbols represent individual mice.

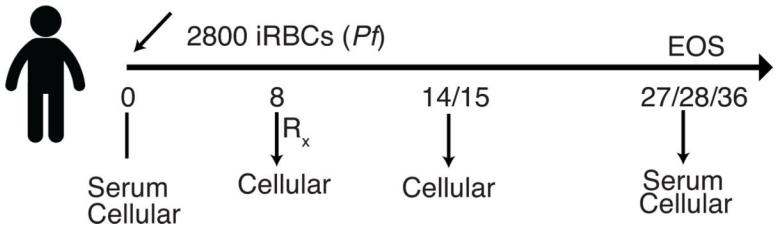

Extended Data Fig. 8. Experimental design for the volunteer infection study

Two thousand eight hundred viable *P. falciparum* infected RBCs were intravenously into malaria naïve healthy volunteers (n = 36 men, n = 4 women). On day 8 p.i., volunteers received anti-malarial drug treatment. On days 0, 8 (treatment day), 14/15 and 27/28/36 (end-of-study, EOS), blood samples were collected and plasmablasts were assessed by flow cytometry.

Supplementary Material

Refer to Web version on PubMed Central for supplementary material.

Acknowldgements

We thank members of the University of Iowa Butler lab for assistance and helpful discussions; F. Lund (University of Alabama, Birmingham) for $\mu s^{-/-}$ mice; T. Honjo (Kyoto University) for *Aicda*$^{-/-}$ mice; T. Waldschmidt (University of Iowa) for clone MR-1 antibody; J. Harty and S. Perlman (University of Iowa) for critical reading of the manuscript and helpful discussions; A. Pewa, E. Taylor and A. Rauckhorst (University of Iowa) for assistance with metabolic measurements; G. Beuttener and B. Wagner (University of Iowa) for metabolic flux assays; and members of the University of Iowa Flow Cytometry Facility for cell sorting. Research in reported in this publication was supported by the NCI (grant no. P30CA086862) and by the National Center for Research Resources of the NIH (grant no. S10OD016199). J.J.G. was supported by a Predoctoral Fellowship from the American Heart Association (grant no. 16PRE27660002). F.A.S. was supported by the NIH (grant no. T32 AI007485. K.J.R. was supported by the NIH (T32 GM067795) W.J.M. was supported by the NIH (grant nos. AI134733 and AI139902). H.-H.X. was supported by the NIH (grant nos. AI121080 and AI139874) and the Veteran Affairs BLR&D Merit Review Program (BX002903). C.R.E. was supported by NHMRC Senior Research Fellowship (grant no. 1154265) and NHMRC Program grant (grant no. 1132975). J.S.M. was also supported by NHMRC Program grant (grant no. 1132975) and a NHMRC Practitioner Fellowship (grant no. 1135955). M.J.B. was supported by NHMRC Career Development Fellowship (grant no. 1141632) and NHMRC Project Grant (grant no.1141278). N.S.B. was supported by the NIH (grant nos. AI125446, AI127481, and AI139902). We thank the participants involved in the malaria volunteer infection studies, Q-Pharm staff, and Medicine for Malaria Venture for funding the clinical trials.

References

1. Nutt SL, Hodgkin PD, Tarlinton DM & Corcoran LM The generation of antibody-secreting plasma cells. Nat Rev Immunol 15, 160–171 (2015). [PubMed: 25698678]
2. Inoue T, Moran I, Shinnakasu R, Phan TG & Kurosaki T Generation of memory B cells and their reactivation. Immunol Rev 283, 138–149 (2018). [PubMed: 29664566]
3. Martin F, Oliver AM & Kearney JF Marginal zone and B1 B cells unite in the early response against T-independent blood-borne particulate antigens. Immunity 14, 617–629 (2001). [PubMed: 11371363]
4. Racine R, Chatterjee M & Winslow GM CD11c expression identifies a population of extrafollicular antigen-specific splenic plasmablasts responsible for CD4 T-independent antibody responses during intracellular bacterial infection. Journal of immunology 181, 1375–1385 (2008).
5. Slifka MK, Antia R, Whitmire JK & Ahmed R Humoral immunity due to long-lived plasma cells. Immunity 8, 363–372 (1998). [PubMed: 9529153]
6. WHO. World malaria report 2018. Geneva: World Health Organization; 2018 https://www.who.int/malaria/publications/world-malaria-report-2018/en/

7. Cohen S, Mc GI & Carrington S Gamma-globulin and acquired immunity to human malaria. Nature 192, 733–737 (1961). [PubMed: 13880318]
8. Changrob S et al. Persistence of Long-lived Memory B Cells specific to Duffy Binding Protein in individuals exposed to Plasmodium vivax. Sci Rep 8, 8347 (2018). [PubMed: 29844379]
9. Longley RJ et al. Naturally acquired antibody responses to more than 300 Plasmodium vivax proteins in three geographic regions. PLoS Negl Trop Dis 11, e0005888 (2017). [PubMed: 28892517]
10. Ndungu FM et al. Long-lived Plasmodium falciparum specific memory B cells in naturally exposed Swedish travelers. Eur J Immunol 43, 2919–2929 (2013). [PubMed: 23881859]
11. Crompton PD et al. A prospective analysis of the Ab response to Plasmodium falciparum before and after a malaria season by protein microarray. Proc Natl Acad Sci U S A 107, 6958–6963 (2010). [PubMed: 20351286]
12. Tran TM et al. An intensive longitudinal cohort study of Malian children and adults reveals no evidence of acquired immunity to Plasmodium falciparum infection. Clin Infect Dis 57, 40–47 (2013). [PubMed: 23487390]
13. Obeng-Adjei N et al. Circulating Th1-Cell-type Tfh Cells that Exhibit Impaired B Cell Help Are Preferentially Activated during Acute Malaria in Children. Cell Rep 13, 425–439 (2015). [PubMed: 26440897]
14. Kurup SP et al. Regulatory T cells impede acute and long-term immunity to blood-stage malaria through CTLA-4. Nat Med 23, 1220–1225 (2017). [PubMed: 28892065]
15. Walther M et al. Upregulation of TGF-beta, FOXP3, and CD4+CD25+ regulatory T cells correlates with more rapid parasite growth in human malaria infection. Immunity 23, 287–296 (2005). [PubMed: 16169501]
16. Weiss GE et al. Atypical memory B cells are greatly expanded in individuals living in a malaria-endemic area. Journal of immunology 183, 2176–2182 (2009).
17. Obeng-Adjei N et al. Malaria-induced interferon-gamma drives the expansion of Tbethi atypical memory B cells. PLoS Pathog 13, e1006576 (2017). [PubMed: 28953967]
18. Portugal S et al. Malaria-associated atypical memory B cells exhibit markedly reduced B cell receptor signaling and effector function. Elife 4 (2015) 15;4:e07218 DOI: 10.7554/eLife.07218.
19. Sullivan RT et al. FCRL5 Delineates Functionally Impaired Memory B Cells Associated with Plasmodium falciparum Exposure. PLoS Pathog 11, e1004894 (2015). [PubMed: 25993340]
20. Ryg-Cornejo V et al. Severe Malaria Infections Impair Germinal Center Responses by Inhibiting T Follicular Helper Cell Differentiation. Cell Rep 14, 68–81 (2016). [PubMed: 26725120]
21. Keitany GJ et al. Blood Stage Malaria Disrupts Humoral Immunity to the Pre-erythrocytic Stage Circumsporozoite Protein. Cell Rep 17, 3193–3205 (2016). [PubMed: 28009289]
22. Butler NS et al. Therapeutic blockade of PD-L1 and LAG-3 rapidly clears established blood-stage Plasmodium infection. Nat Immunol 13, 188–195 (2011). [PubMed: 22157630]
23. Horne-Debets JM et al. PD-1 dependent exhaustion of CD8+ T cells drives chronic malaria. Cell Rep 5, 1204–1213 (2013). [PubMed: 24316071]
24. Guthmiller JJ, Graham AC, Zander RA, Pope RL & Butler NS Cutting Edge: IL-10 Is Essential for the Generation of Germinal Center B Cell Responses and Anti-Plasmodium Humoral Immunity. Journal of immunology 198, 617–622 (2017).
25. Krishnamurty AT et al. Somatically Hypermutated Plasmodium-Specific IgM(+) Memory B Cells Are Rapid, Plastic, Early Responders upon Malaria Rechallenge. Immunity 45, 402–414 (2016). [PubMed: 27473412]
26. Shaffer AL et al. Blimp-1 orchestrates plasma cell differentiation by extinguishing the mature B cell gene expression program. Immunity 17, 51–62 (2002). [PubMed: 12150891]
27. William J, Euler C & Shlomchik MJ Short-lived plasmablasts dominate the early spontaneous rheumatoid factor response: differentiation pathways, hypermutating cell types, and affinity maturation outside the germinal center. Journal of immunology 174, 6879–6887 (2005).
28. Tellier J et al. Blimp-1 controls plasma cell function through the regulation of immunoglobulin secretion and the unfolded protein response. Nat Immunol 17, 323–330 (2016). [PubMed: 26779600]

29. Meding SJ, Cheng SC, Simon-Haarhaus B & Langhorne J Role of gamma interferon during infection with Plasmodium chabaudi chabaudi. Infect Immun 58, 3671–3678 (1990). [PubMed: 1977706]
30. Su Z & Stevenson MM Central role of endogenous gamma interferon in protective immunity against blood-stage Plasmodium chabaudi AS infection. Infect Immun 68, 4399–4406 (2000). [PubMed: 10899836]
31. Reimold AM et al. Plasma cell differentiation requires the transcription factor XBP-1. Nature 412, 300–307 (2001). [PubMed: 11460154]
32. Boothby M & Rickert RC Metabolic Regulation of the Immune Humoral Response. Immunity 46, 743–755 (2017). [PubMed: 28514675]
33. Cantor J et al. CD98hc facilitates B cell proliferation and adaptive humoral immunity. Nat Immunol 10, 412–419 (2009). [PubMed: 19270713]
34. Cordy RJ et al. Distinct amino acid and lipid perturbations characterize acute versus chronic malaria. JCI Insight 4 (2019). 4(9):e125156 10.1172/jci.insight.125156
35. Suan D et al. CCR6 Defines Memory B Cell Precursors in Mouse and Human Germinal Centers, Revealing Light-Zone Location and Predominant Low Antigen Affinity. Immunity 47, 1142–1153 e1144 (2017). [PubMed: 29262350]
36. Alugupalli KR et al. B1b lymphocytes confer T cell-independent long-lasting immunity. Immunity 21, 379–390 (2004). [PubMed: 15357949]
37. Haas KM, Poe JC, Steeber DA & Tedder TF B-1a and B-1b cells exhibit distinct developmental requirements and have unique functional roles in innate and adaptive immunity to S. pneumoniae. Immunity 23, 7–18 (2005). [PubMed: 16039575]
38. Pelletier N et al. Plasma cells negatively regulate the follicular helper T cell program. Nat Immunol 11, 1110–1118 (2010). [PubMed: 21037578]
39. Khan AR et al. PD-L1hi B cells are critical regulators of humoral immunity. Nat Commun 6, 5997 (2015). [PubMed: 25609381]
40. Matsumoto M et al. Interleukin-10-producing plasmablasts exert regulatory function in autoimmune inflammation. Immunity 41, 1040–1051 (2014). [PubMed: 25484301]
41. Clark EH et al. Plasmodium falciparum malaria in the Peruvian Amazon, a region of low transmission, is associated with immunologic memory. Infect Immun 80, 1583–1592 (2012). [PubMed: 22252876]
42. Labak CM et al. Glucose transport: meeting the metabolic demands of cancer, and applications in glioblastoma treatment. Am J Cancer Res 6, 1599–1608 (2016). [PubMed: 27648352]
43. Lam WY et al. Metabolic and Transcriptional Modules Independently Diversify Plasma Cell Lifespan and Function. Cell Rep 24, 2479–2492 e2476 (2018). [PubMed: 30157439]
44. Chapuis N, Poulain L, Birsen R, Tamburini J & Bouscary D Rationale for Targeting Deregulated Metabolic Pathways as a Therapeutic Strategy in Acute Myeloid Leukemia. Front Oncol 9, 405 (2019). [PubMed: 31192118]
45. Zhu X, Pan Y, Li Y, Cui L & Cao Y Supplement of L-Arg improves protective immunity during early-stage Plasmodium yoelii 17XL infection. Parasite Immunol 34, 412–420 (2012). [PubMed: 22709481]
46. Gordon EB et al. Targeting glutamine metabolism rescues mice from late-stage cerebral malaria. Proc Natl Acad Sci U S A 112, 13075–13080 (2015). [PubMed: 26438846]
47. Miyakoda M et al. Malaria-specific and nonspecific activation of CD8+ T cells during blood stage of Plasmodium berghei infection. Journal of immunology 181, 1420–1428 (2008).

Methods-only References

48. McCarthy JS et al. A pilot randomised trial of induced blood-stage Plasmodium falciparum infections in healthy volunteers for testing efficacy of new antimalarial drugs. PLoS One 6, e21914 (2011). [PubMed: 21887214]
49. Rockett RJ et al. A real-time, quantitative PCR method using hydrolysis probes for the monitoring of Plasmodium falciparum load in experimentally infected human volunteers. Malar J 10, 48 (2011). [PubMed: 21352599]

50. Collins KA et al. A controlled human malaria infection model enabling evaluation of transmission-blocking interventions. J. Clin. Invest 128, 1551–1562 (2018). [PubMed: 29389671]

51. Montes de Oca M et al. Type I Interferons Regulate Immune Responses in Humans with Blood-Stage Plasmodium falciparum Infection. Cell Rep 17, 399–412 (2016). [PubMed: 27705789]

52. Malleret B et al. A rapid and robust tri-color flow cytometry assay for monitoring malaria parasite development. Sci Rep 1, 118 (2011). [PubMed: 22355635]

53. Villarino NF et al. Composition of the gut microbiota modulates the severity of malaria. Proc Natl Acad Sci U S A 113, 2235–2240 (2016). [PubMed: 26858424]

54. Dobin A et al. STAR: ultrafast universal RNA-seq aligner. Bioinformatics 29, 15–21 (2013). [PubMed: 23104886]

55. Liao Y, Smyth GK & Shi W featureCounts: an efficient general purpose program for assigning sequence reads to genomic features. Bioinformatics 30, 923–930 (2014). [PubMed: 24227677]

56. Gray LR et al. Hepatic Mitochondrial Pyruvate Carrier 1 Is Required for Efficient Regulation of Gluconeogenesis and Whole-Body Glucose Homeostasis. Cell Metab 22, 669–681 (2015). [PubMed: 26344103]

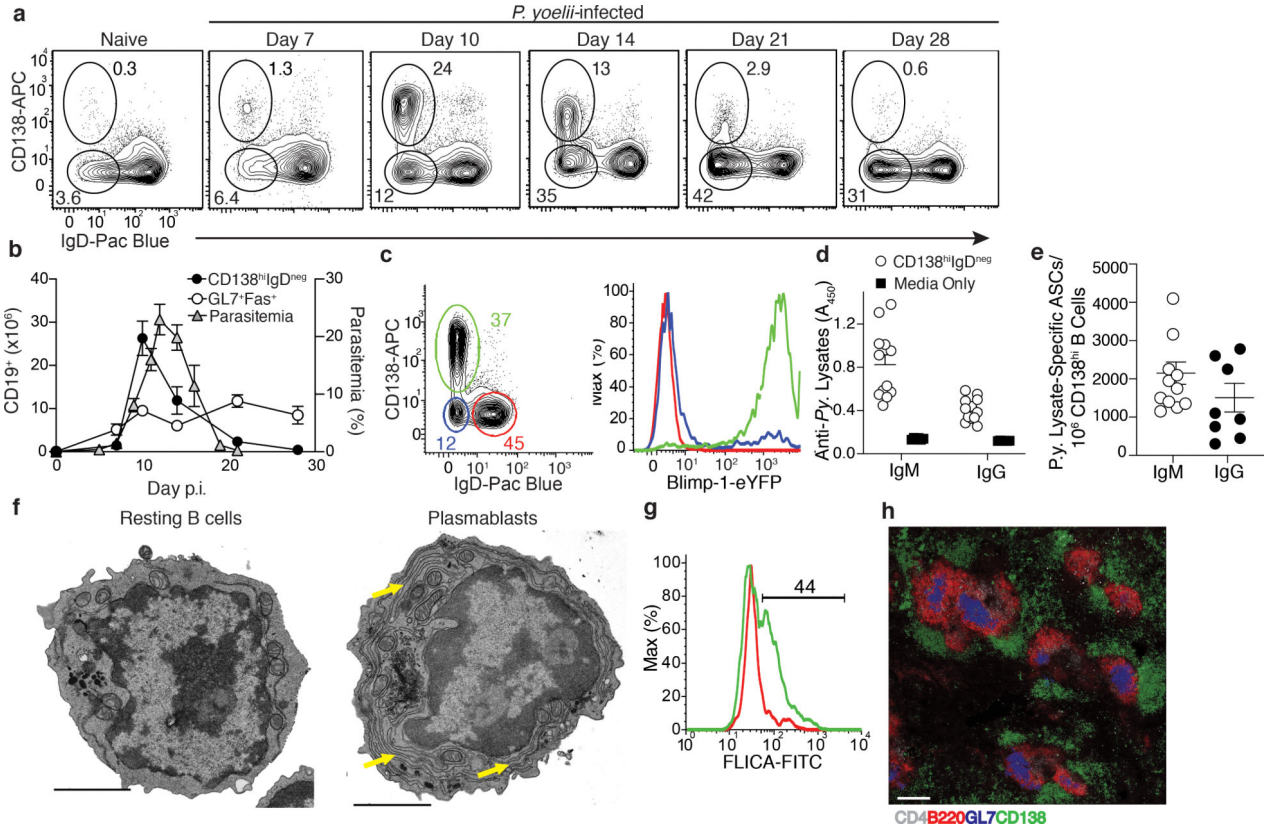

Fig. 1. Preferential expansion of plasmablasts during experimental malaria.

a, Plots showing kinetics of splenic CD138^{hi}IgD^{neg} B cells, representative of 6 biologically independent experiments with similar results. **b,** Numbers of splenic plasmablasts (CD138^{hi}IgD^{neg}), GC B cells (GL7^{+}Fas^{+}) and kinetics of parasite burden (% of infected red blood cells) during *Py* infection. Data are means ± s.d. and representative of $n = 3$ biologically independent experiments with similar results using $n = 5$ (PB and GC B cells) and n = 4 mice (parasitemia). **c**, Blimp-1-eYFP expression among CD138^{hi}IgD^{neg} (green), CD138^{lo}IgD^{neg} (blue) and CD138^{lo}IgD^{hi} (red) cells on day 10 p.i. Data are representative of $n = 2$ independent experiments with $n = 8$ mice. **d**, Parasite-specific IgM and IgG antibody secreted by splenic CD138^{hi}IgD^{neg} plasmablasts isolated on day 10 p.i. Data are means ± s.e.m., pooled from 2 biologically independent experiments with $n = 6$ wells (media only) wells and $n = 12$ wells (CD138^{hi}IgD^{neg}). **e**, Numbers of parasite-specific antibody secreting CD138^{hi}IgD^{neg} plasmablasts isolated on day 10 p.i. Data are means ± s.e.m., pooled from n = 2 biologically independent experiments with $n = 8$ (IgG) and $n = 11$ mice (IgM). **f**, Transmission electron micrographs of indicated cells isolated on day 10 p.i. Data representative of $n = 3$ biologically independent experiments with similar results using $n =$ 100 cells for each population and 1 mouse/experiment. Scale bar, 2 μm. Yellow arrows, rough endoplasmic reticulum. **g**, FLICA staining in CD138^{hi}IgD^{neg} plasmablasts (green) and naïve B cells (red) on day 10 p.i. Data representative of $n = 2$ biologically independent experiments similar results using $n = 6$ mice/time point. **h**, Confocal micrographs of day 10 p.i. spleen showing CD4 T cells (gray), total B cells (red), germinal center B cells (blue) and

CD138^{hi} plasmablasts (green). Data representative of $n = 2$ biologically independent experiments using $n = 3$ mice. Scale bar, 300μm.

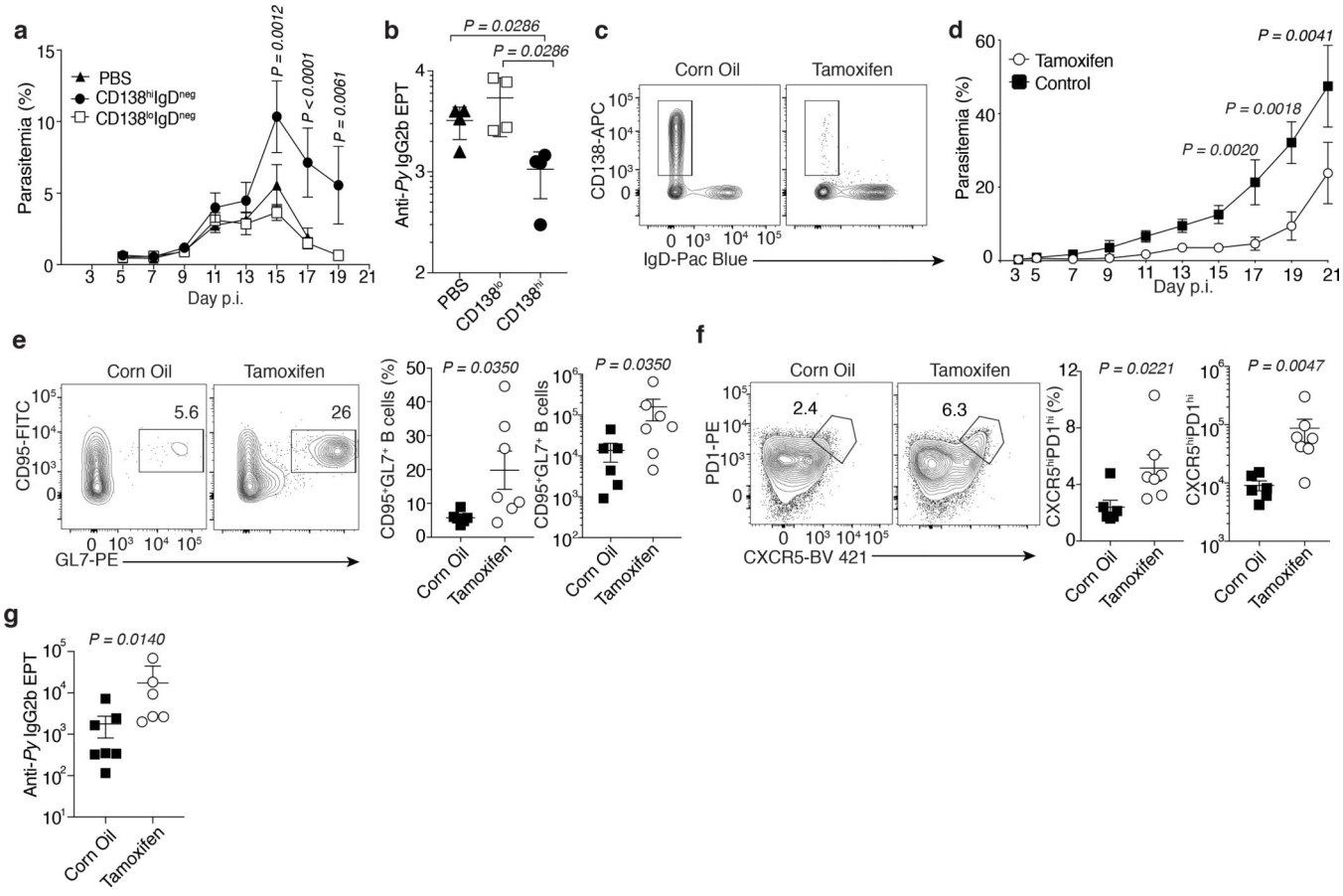

Fig. 2. Blocking plasmablast development improves humoral immunity.

a,**b**, *Py*-infected mice were transferred either CD138^{hi}IgD^{neg} plasmablasts, CD138^{lo}IgD^{neg} activated B cells or PBS. Kinetics of parasite burden (**a**) and anti-parasite IgG2b serum antibody endpoint titers (EPT) on day 21 p.i (**b**) in recipients. Data in a are means ± s.e.m pooled from $n = 2$ independent experiments with $n = 7$ (IgD^{neg}CD138^{hi}) and n = 8 (IgD^{neg}CD138^{lo} and PBS) mice analyzed by two-way ANOVA with Tukey's multiple comparison test (DF = 14; F = 2.603). Data in b are means ± s.d. and representative of $n = 2$ biologically independent experiments with similar results using $n = 4$ mice/group. **c**-**g**, Rosa26-ERT2/Cre *Prdm1*$^{fl/fl}$: μMT bone marrow chimeras infected with *Py* were either treated with vehicle (corn oil) or tamoxifen on days 4, 5 and 6 p.i. Plots showing abrogation of plasmablasts on day 10 p.i. (**c**) and kinetics of parasite burden (**d**). Data are means ± s.e.m, pooled from $n = 2$ independent experiments with $n = 6$ mice/group. **e**-**g**, Numbers of splenic GC B cells (**e**), GC-T$_{FH}$-like cells (**f**) and anti-*Py* serum antibody EPT (**g**) on day 21 p.i. Data are means ± s.e.m., pooled from $n = 2$ biologically independent experiments with $n = 6$ (corn oil) and $n = 7$ mice (tamoxifen). For d, data were analyzed using two-way ANOVA with Sidak's multiple comparison test (DF= 9; F= 3.1). For b,e,f, and g, two-tailed Mann-Whitney tests were used for statistical analyses. Symbols in b, e-g represent individual mice.

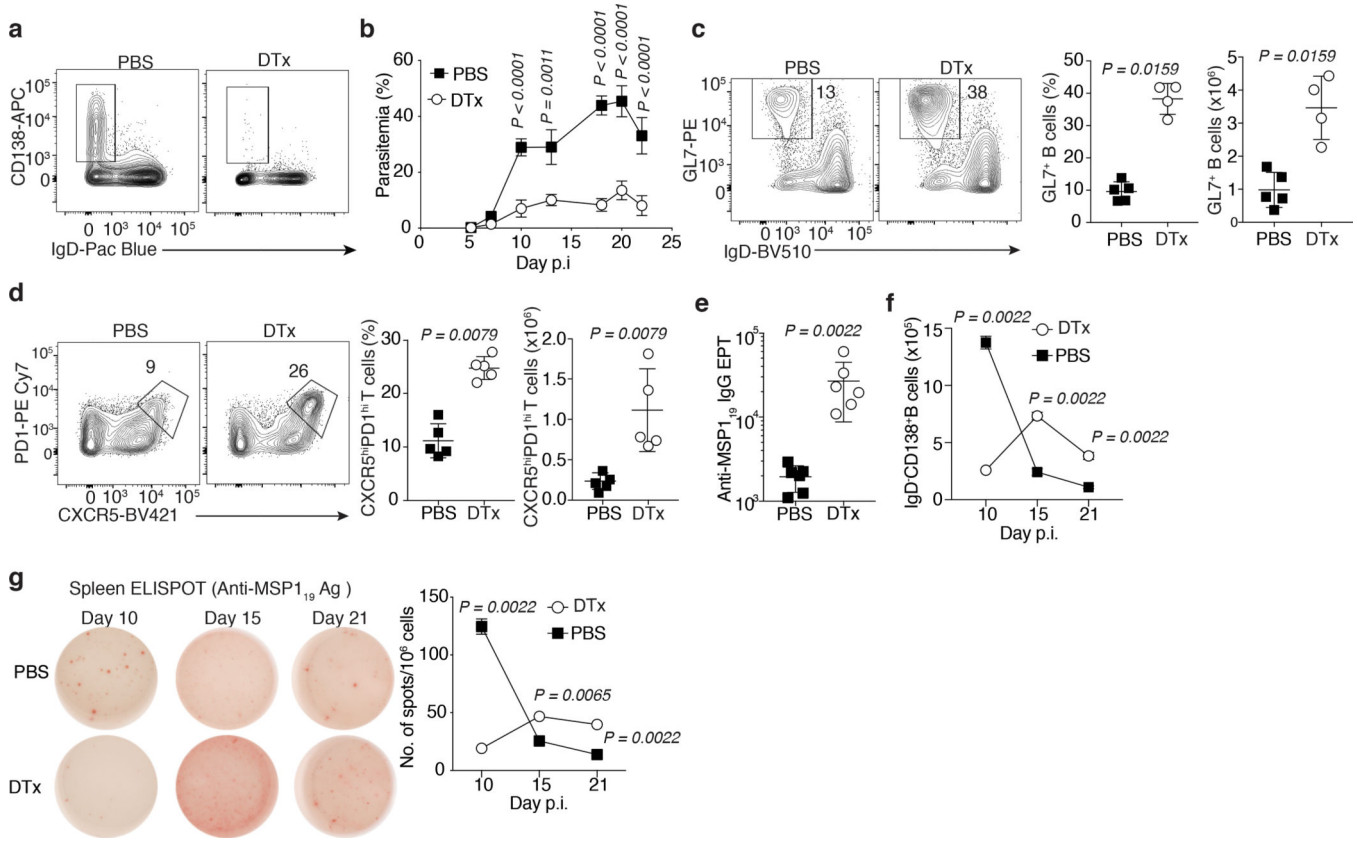

Fig. 3. Deletion of plasmablasts enhances humoral immunity.

a-g, CD138-DTR bone marrow chimeras were infected with *Py* and treated with either vehicle (PBS) or diphtheria toxin (DTx) on days 5 and 7 p.i. Plots showing deletion of plasmablasts on day 10 p.i (**a**) and kinetics of parasite burden (**b**). Data are means ± s.e.m, pooled from $n = 2$ biologically independent experiments with $n = 7$ mice/group analyzed with a two-way ANOVA with Sidak's multiple comparison test (DF = 6; F = 8.777). **c**, Numbers of splenic GC B cells. Data are means ± s.d. representative of $n = 2$ biologically independent experiments with similar results using $n = 5$ (PBS) and $n = 4$ mice (DTx). **d,** Numbers of splenic GC-T_{FH}-like cells. Data are means ± s.d. representative of $n = 2$ biologically independent experiments with similar results using $n = 5$ mice/group. **e**, Anti-$MSP1_{19}$ specific serum antibody EPT on day 21 p.i. Splenic plasmablast kinetics as detected by flow cytometry (**f**) and ELISPOT (**g**). Data in e-g are means ± s.e.m., pooled from $n = 2$ biologically independent experiments with $n = 6$ mice/group. Symbols in c-e represent individual mice. For panels c-g, data were analyzed using two-tailed Mann-Whitney.

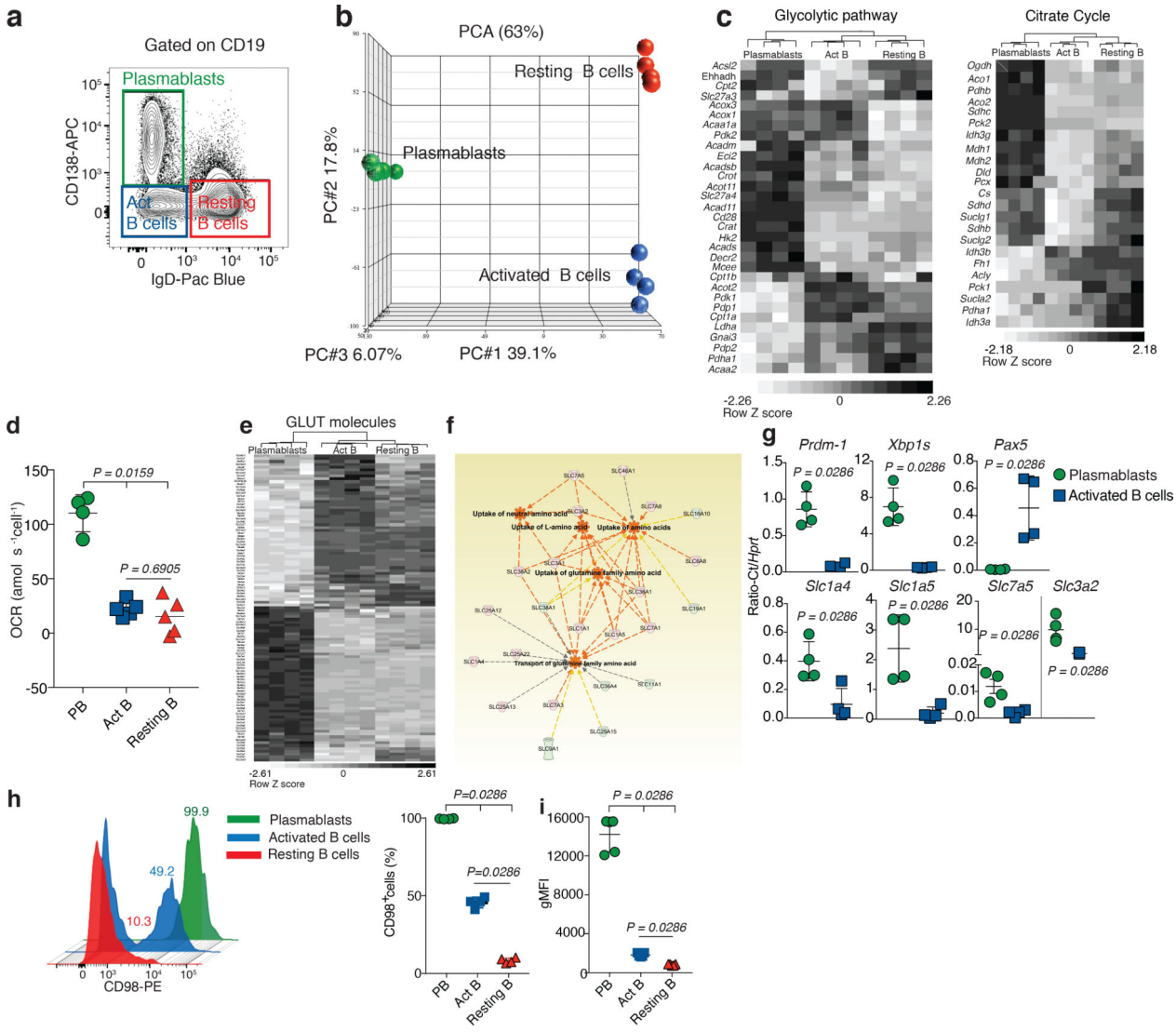

Fig. 4. Plasmablasts are metabolically hyperactive.

a, Gating strategy used for sorting plasmablasts and activated and resting B cell populations from *Py*-infected mice on day 10 p.i. that were used for bulk RNA-sequencing. **b**,**c**, Principal component analysis (PCA) depicting the clustering of transcriptomic data set from the three different B cell populations (**b**) and heat maps showing relative expression levels of different genes involved in glycolytic pathway (**c**, left) and citrate cycle pathway (**c**, right). **d**, Data comparing basal respiration of the three splenic B cell populations sort-purified from *Py*-infected mice on day 10 p.i. Data are means ± s.e.m. for $n = 4$ technical replicates, representative of $n = 3$ biologically independent experiments with similar results with $n = 4$ wells/cell type and analyzed by one-way ANOVA followed by Tukey's multiple comparisons test. **e**,**f**, Heat map showing relative expression levels of various GLUT molecules (**e**) and network of various amino acid transporter pathways generated using Ingenuity Pathway Analysis (**f**). **g**, mRNA expression levels (relative to *Hprt*) of plasmablast specific genes (*Prdm1*, *Xbp1s*), B cell lineage gene (*Pax5)* and L-glutamine transporter molecules *Slc1a4*, *Slc1a5*, and *Cd98 (Slc3a2 and Slc7a5)*. Data are means ± s.e.m. for $n = 4$

mice, representative of $n = 2$ biologically independent experiments with similar results using $n = 2$ technical replicates and analyzed by two-tailed Mann-Whitney. **h**, **i**, Frequency (**h**) and geometric mean fluorescence intensity (**i**) of CD98 expression on the indicated B cell populations isolated on day 10 p.i. Data are means ± s.d., representative of $n = 2$ biologically independent experiments with similar results using $n = 4$ mice and analyzed by one-way ANOVA. Symbols in b, d, g, h and i represent individual wells/mice. For panels a-c, e and f, $n = 4$ mice with data acquired from one experiment and analyzed by two-way ANOVA (FDR < 0.05 and fold change < −2 > 2).

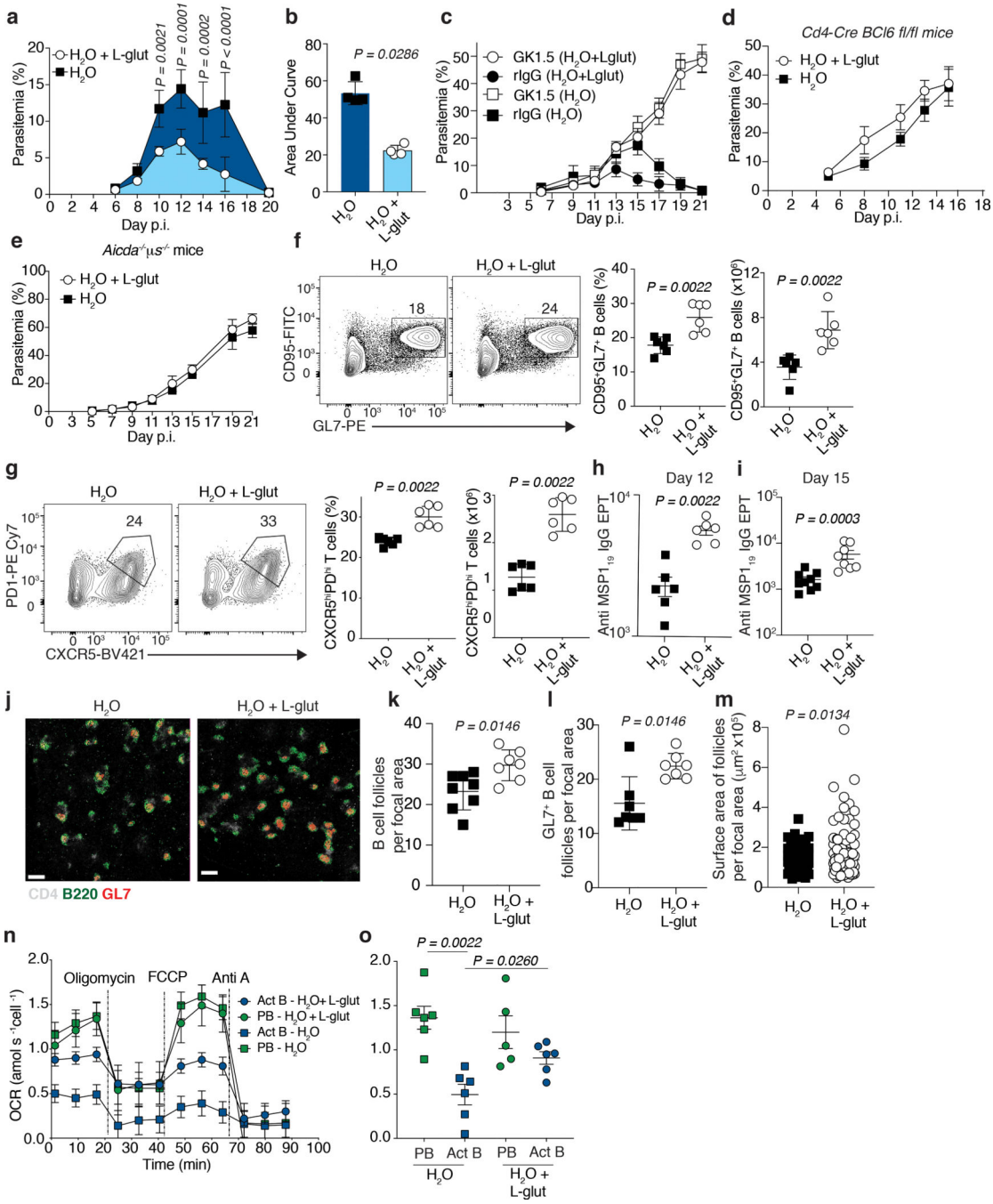

Fig. 5. L-glutamine supplementation enhances germinal center responses.

a-**n**, Mice of the indicated genotypes were either left untreated (H_2O) or treated with L-glutamine supplemented water (H_2O + L-glut) starting on day 0 p.i. **a**,**b**, Kinetics of parasite burden (**a**) and area under curve as a measure of total parasite biomass (**b**). Data are means ± s.d., representative of $n = 3$ biologically independent experiments with similar results using $n = 4$ mice/group. Data in a were analyzed using a two-way ANOVA with Sidak's multiple comparison test (DF = 6; F = 6.542). **c**, Kinetics of parasite burden in wild-type mice treated with either GK1.5 or rIgG on days 5 and 7 p.i. Data are means ± s.e.m., pooled from $n = 2$

biologically independent experiments with $n = 6$ (H_2O+L-glut+GK1.5, H_2O+GK1.5 and H_2O+rIgG) and $n = 7$ mice (H_2O+L-glut+rIgG). **d**, Kinetics of parasite burden in *CD4-Cre x* $Bcl6^{fl/fl}$ mice. Data are means ± s.e.m., pooled from $n = 2$ biologically independent experiments with $n = 7$ mice/group. **e**, Kinetics of parasite burden in $Aicda^{-/-}\mu S^{-/-}$ mice. Data are means ± s.e.m, pooled from $n = 2$ biologically independent experiments with $n = 6$ mice/group. **f**,**g**, Numbers of splenic GC B cells (**f**) and GC-T_{FH}-like cells (**g**) on day 12 p.i. in *Py*-infected mice. Data are means ± s.e.m, pooled from $n = 2$ biologically independent experiments with $n = 6$ mice/group. **h**,**i**, Anti-$MSP1_{19}$ IgG serum titers on days 12 and day 15 p.i. Data in h,i are means ± s.e.m, pooled from $n = 2$ biologically independent experiments with $n = 6$ (h), $n = 9$ (i, H_2O) or $n = 8$ mice mice/group (i, H_2O + L-glut). **j-m**, Confocal micrographs (**j**, scale bars, 500 μm), numbers of B cell follicles (**k,** $n = 8$, H_2O; $n =$ 7 mice, H_2O + L-glut), number of $GL7^+$ B cell follicles (**l**, $n = 7$ mice/group) and the surface area of B cell follicles per focal area (**m**, $n = 58$ foci, H_2O; $n = 78$ foci, H_2O+L-glut) in the spleens of mice on day 12 p.i. Data in k-m are means ± s.e.m, pooled from $n = 2$ biologically independent experiments. **n**,**o**, Oxygen consumption rates (**n**) and basal respiration (**o**, minutes 0–20) of plasmablasts and activated B cells isolated on day 10 p.i. Data in n,o are means ± s.e.m., representative of $n = 2$ biologically independent experiments with similar results using $n = 5$ (PB, H_2O; activated B cells H_2O+L-glut) and $n = 6$ (activated B cells, H_2O; PB, H_2O+L-glut) technical replicates using 2.5×10^5 cells/well sorted from $n = 3$ mice/group. Symbols in b, f, g, h, i, k and l represent individual mice. Symbols in m and o represent technical replicates. Data in m were analyzed using a two-tailed unpaired *t* test ($t = 2.505$, $df = 134$). Data in f, g, h, i, k, l and o were analyzed with two-tailed Mann-Whitney.

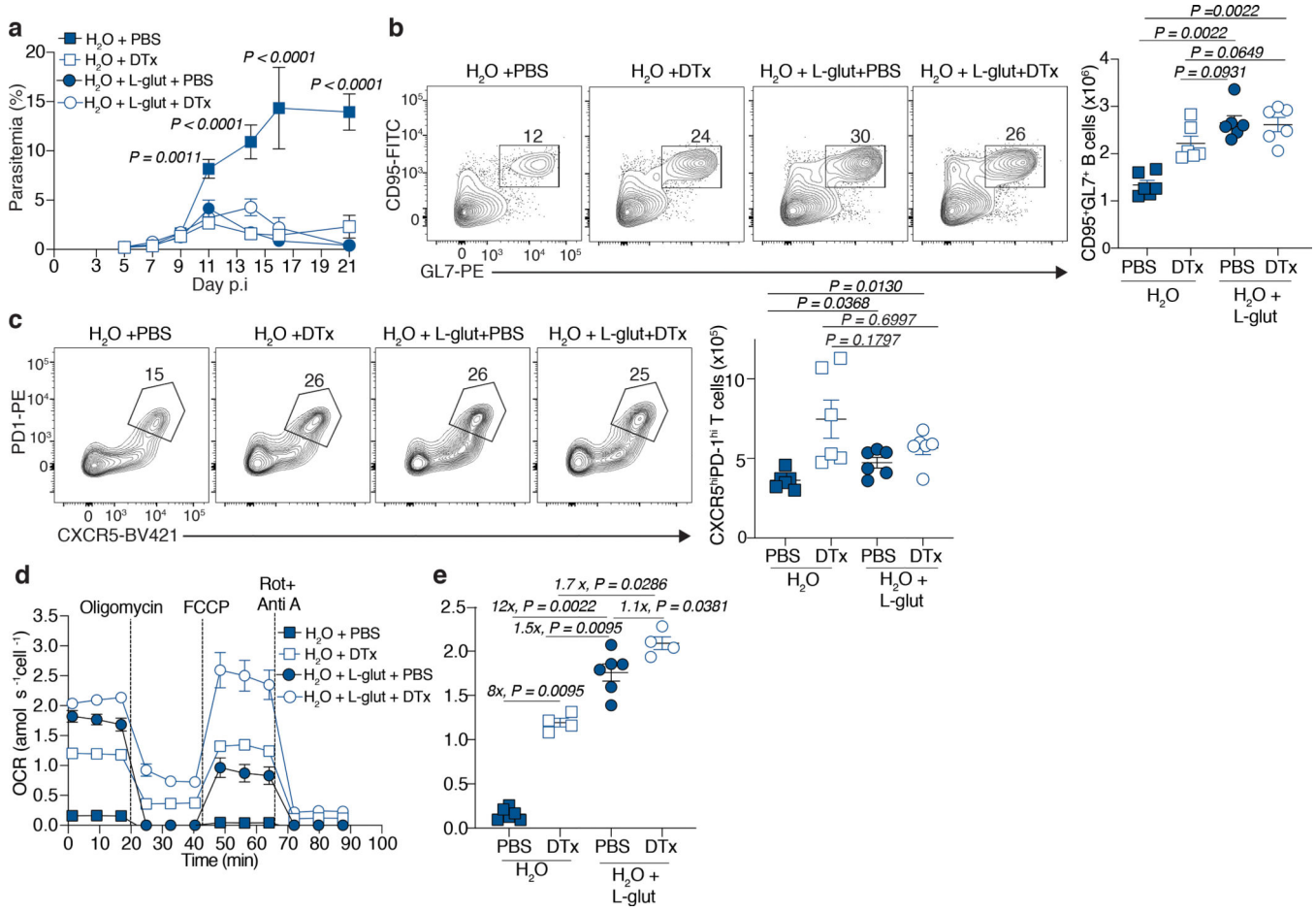

Fig 6. Plasmablast deletion and L-glutamine are functionally redundant.

a-e, *Py*-infected CD138-DTR bone marrow chimeric mice were either left untreated (H_2O) or treated with L-glutamine supplemented water (H_2O + L-glut) starting on day 0 p.i. Mice were subsequently treated with either vehicle (PBS) or diphtheria toxin (DTx) on days 5 and 7 p.i. Kinetics of parasite burden (**a**) and numbers of splenic GC B cells (**b**) and GC-T_{FH}-like cells (**c**) on day 21 p.i. Data are mean ± s.e.m, pooled from 2 biologically independent experiments with $n = 6$ mice/group. Oxygen consumption rates (OCR) of activated B cells isolated from indicated groups on day 10 p.i. (**d**) and summary graph of basal respiration (**e**, minutes 0–20) among treatment groups. Data are means ± s.e.m., representative of $n = 2$ biologically independent experiments with similar results using $n = 4$ (H_2O+DTx and H_2O +L-glut+DTx) and $n = 6$ technical replicates (H_2O+PBS and H_2O+L-glut+PBS) with $2.5 \times 10^5 – 1 \times 10^6$ cells/well sorted from $n = 4$ mice per group. Symbols in b and c represent individual mice. Symbols in e represent technical replicates. Data were analyzed with either a two-way ANOVA with Tukey post hoc test (a, DF = 18; F = 8.789) or two-tailed Mann Whitney (b-d).

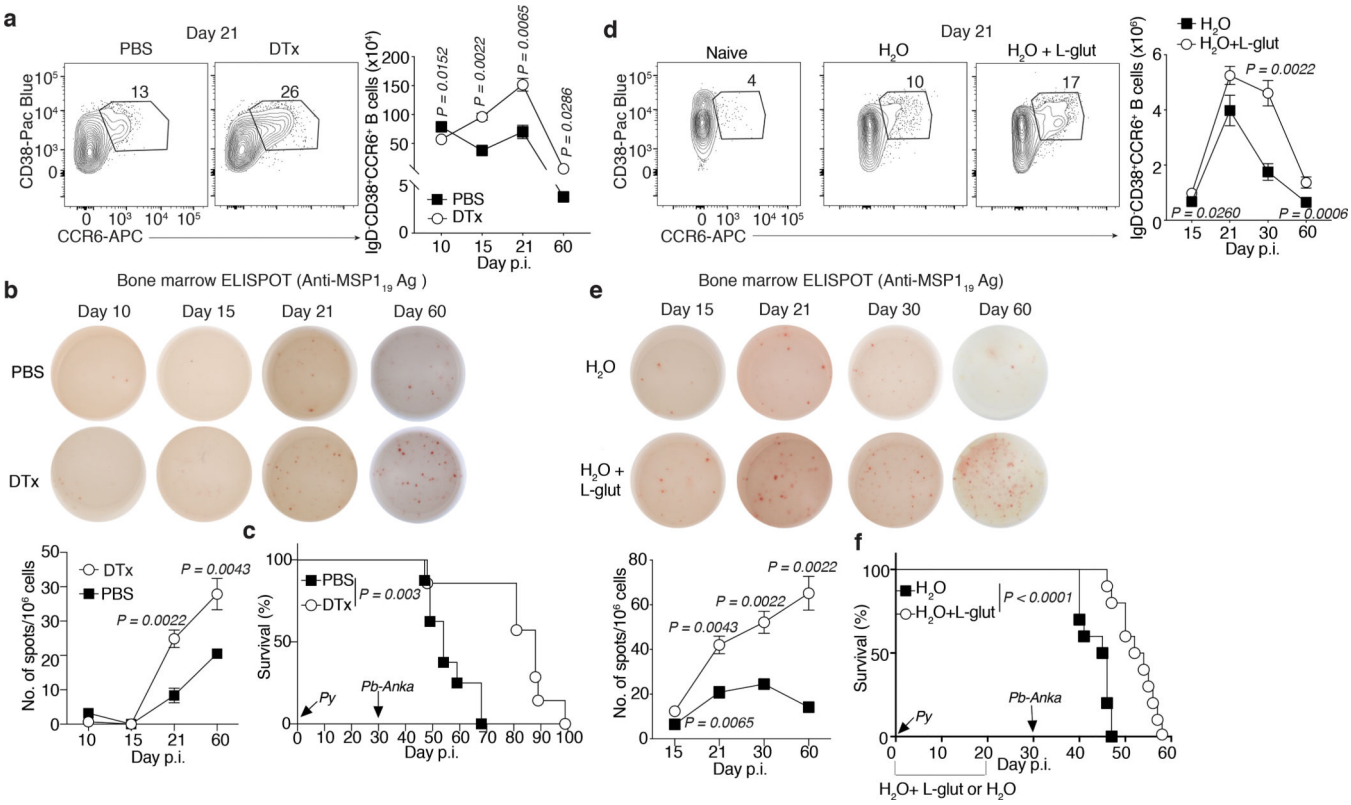

Fig 7. Plasmablast deletion and L-glutamine enhance humoral immune memory.

a-c, *Py*-infected CD138-DTR bone marrow chimeras were treated with vehicle (PBS) or diphtheria toxin (DTx) on days 5 and 7 p.i. Kinetics of splenic memory B cells (**a**) and bone marrow antibody-secreting cells (**b**). Data in a,b are means ± s.e.m., pooled from $n = 2$ biologically independent experiments with $n = 4$ (day 60) and $n = 6$ mice/group (days 10, 15 and 21). **c**, Survival of mice challenged with *Pb-Anka* 30 days after an initial *Py* infection. Data are pooled from 2 biologically independent experiments with $n = 7$ (DTx) and $n = 8$ mice (PBS). **d-f**, *Py*-infected wild-type mice were either left untreated (H_2O) or treated with L-glutamine supplemented water (H_2O + L-glut) starting on day 0 p.i. **d**, Kinetics of splenic memory B cell responses. **e**, Kinetics of bone marrow antibody-secreting cells. Data in d,e are means ± s.e.m., pooled from $n = 2$ biologically independent experiments with $n = 6$ mice/group. **f**, Survival of mice challenged with *Pb-Anka* 30 days after an initial *Py* infection. Data are pooled from $n = 2$ independent experiments with $n = 10$ mice/group. Data in a, b, d, and e, were analyzed with two-tailed Mann Whitney. Data in c and f were analyzed with Mantel-Cox.

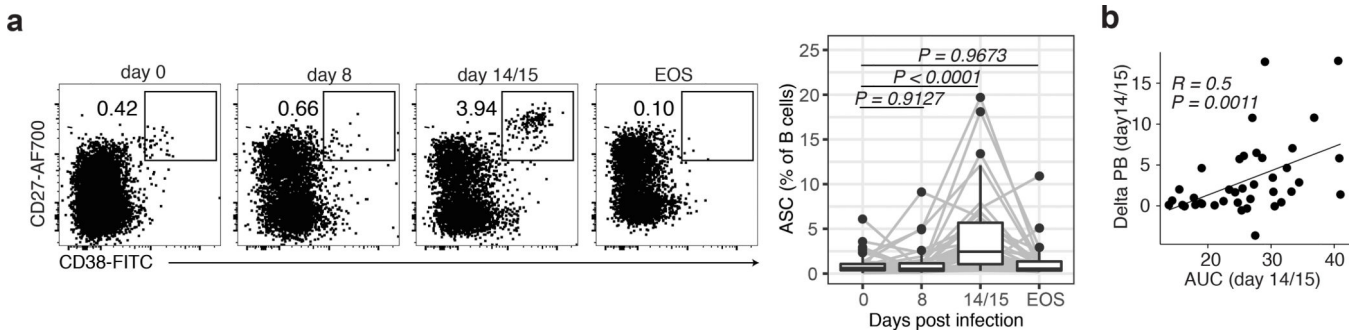

Fig 8. Positive correlation between parasite burden and plasmablasts in human malaria.

a, Plots (left panel, gated on $CD19^{+}CD3^{-}$ cells) and summary graph (right panel) showing the kinetics of plasmablasts in the peripheral blood of volunteers drawn on the indicated days during the course of the study. Boxplots are median ± IQR, whiskersare data range to 1.5 × IQR analyzed by two-sided Wilcoxon matched-pairs signed rank tests. **b**, Correlation graph showing the relationship between parasite burden on day 15 (area under curve, AUC) and the increase in plasmablasts numbers from day 0 to day 15 (delta PB-day 15). Data were analyzed by two-tailed Spearmans rho. Data in a,b derive from $n = 36$ men and $n = 4$ women from 4 studies across 6 independent cohorts.